Investigating the role of TMED2 in murine embryonic liver development

Wesley Chan

Department of Anatomy and Cell Biology

McGill University

Montreal, QC, Canada

December 2018

A thesis submitted to McGill University in partial fulfillment of the requirements of the degree of Master of Science

PREFACE

All experimental procedures and analyses presented in this thesis titled "Investigating the role of TMED2 in murine embryonic liver development" were performed by me (Wesley Chan), the author, unless otherwise indicated. The project presented in this thesis was conceptualized and developed with the supervision of Dr. Loydie A. Jerome-Majewska, my thesis supervisor. The thesis was written and prepared by myself in accordance to the McGill University's thesis preparation guidelines.

ABSTRACT

TMED2 is a member of the transmembrane emp24 domain-containing (TMED) cargo receptors involved in trafficking proteins within the secretory pathway. It is expressed in mouse livers throughout development. *Tmed2*$^{99J/99J}$ embryos lacking TMED2 die by embryonic day (E) 11.5. In contrast, though *Tmed2*$^{99J/+}$ mice expressing lower levels of TMED2 survive until adulthood, a significant number develop non-alcoholic fatty liver disease after 6 months of age. Thus, we hypothesize that TMED2 is required during embryonic and post-natal liver development. Analysis of HE-stained liver sections revealed reduced erythrocyte and increased granulocyte proportions relative to all cells in E17.5 *Tmed2*$^{99J/+}$ livers. However, complete blood count analysis of peripheral blood of 3 month old *Tmed2*$^{99J/+}$ mice revealed no change in blood cell count compared to wild-type controls. Differences in cell proportion at E17.5 were not associated with differences in expression of key hematopoietic transcription factors associated with various hematopoietic progenitors in E14.5 livers using RT-qPCR. No defects in clotting was observed in *Tmed2*$^{99J/+}$mice. All in all, other than a deregulated cell proportion observed at E17.5, *Tmed2*$^{99J/+}$animals do not appear to present with developmental defects in the liver. Concomitantly, since *Tmed2*$^{99J/+}$embryonic lethality precludes the study of these embryos, we are generating *Tmed2*$^{fl/fl}$ mice containing loxP-flanked *Tmed2* exon 2 using CRISPR/Cas9-mediated homology-directed repair technology. Thus far, a loxP site was successfully introduced into *Tmed2* intron 1.

RÉSUMÉ

TMED2 fait partie de la famille de protéines « transmembrane emp24 domain-containing » (TMED). Les membres de la famille TMED fonctionnent comme récepteurs transmembranaires au cours du traffic intra-cellulaire des protéines entre le réticulum endoplasmique (RE) et l'appareil de Golgi. Le gène *Tmed2* est exprimé par le foie pour la durée du développement embryonnaire murin. Les embryons murin $Tmed2^{99J/99J}$, qui ne produit pas de TMED2, ne survivent pas après le 11,5e jour de l'embryogenèse (E11,5) à cause des anomalies de la formation du placenta. Au contraire, les souris hétérozygotes de *Tmed2* sont viables et fertiles mais elles ont une augmentation d'incidence de « non-alcoholic fatty liver disease » (NAFLD) à partir de l'âge de 6 mois. Notre hypothèse est que TMED2 est nécessaire pendant le développement hépatique embryonnaire et postnatal. Des analyses histologiques ont révélé que les foies des embryons *Tmed2* hétérozygotes E17,5 ont une proportion accrue d'érythrocytes et une diminution de la proportion de granulocytes. Cependant, nous n'avons pas observé cette différence dans le sang périphérique de souris âgées de 3 mois par une analyse du sang appelée hémogramme. De plus, nous n'avons pas observé de différence de l'expression des facteurs de transcriptions associés au développement des progéniteurs hématopoïétiques dans le foie des souris *Tmed2* hétérozygotes E14,5 par RT-qPCR. Aucune anomalie de coagulation du sang des souris *Tmed2* hétérozygotes n'a été détecté. Globalement, hormis une proportion de cellules déréglementées observée à E17,5, les animaux hétérozygotes de *Tmed2* ne semblent pas présenter de défauts de développement du foie. En parallèle, puisque les embryons *Tmed2* homozygotes meurent au stade mi-embryonnaire, nous générons, à l'aide de la technique de CRISPR/Cas9, des souris $Tmed2^{fl/fl}$ dans lesquelles l'exon 2 de *Tmed2* est flanqué par deux sites loxP. Jusqu'à présent, nous avons introduit avec succès un site loxP dans l'intron 1 de *Tmed2*.

ACKNOWLEDGEMENTS

First and foremost, I would like to thank Dr. Loydie A. Jerome-Majewska for giving me the wonderful opportunity of working and studying in her laboratory. Without her extraordinary patience, care and devotion I would not have learned as much as I have and this thesis would not have been possible. Her knowledge and guidance has significantly contributed to my professional growth as a researcher-in-training but also my personal growth.

I would also like to thank the members of the Majewska lab Dr. Marie-Claude Beauchamp, Dr. Dominic Hou, Sabrina Alam and Vafa Keiser for teaching me many laboratory techniques and for providing endless support during stressful times. I will never forget all the laughter and joyful moments that we shared.

My thesis would also not have been possible without the helpful feedback and guidance from my Advisory Committee: Dr. Natalie Lamarche-Vane, Dr. Christian Rocheleau and Dr. Yojiro Yamanaka.

I would like to extend my gratitude to my friends whom have embarked on the same graduate school journey. Their support and compassion have been tremendously helpful and encouraging.

Lastly, pertaining specifically to the preparation of this thesis, I would like to thank Dr. Jerome-Majewska for her guidance and valuable feedback. I would also like to thank Moushumi Nath and Xinwen Zhu for proof-reading my thesis and providing helpful commentary. Last but not least, I would like to thank Dr. Beauchamp for proof-reading the French translation of my abstract.

TABLE OF CONTENTS

LIST OF TABLES AND FIGURES

ABBREVIATIONS

ANOVA	analysis of variance
BMP	bone morphogenic protein
cDNA	complementary DNA
CGN	cis-Golgi network
cKO	conditional knock-out
CO_2	carbon dioxide
COP	coat-protein
CRISPR	clustered regularly interspaced short palindromic repeats
ddH_2O	double distilled water
DEPC	diethyl pyrocarbonate
DNA	deoxyribonucleic acid
DSB	double-stranded break
EDTA	ethylenediaminetetraacetic acid
ER	endoplasmic reticulum
ERGIC	ER-to-golgi intermediate compartment
EtOH	ethanol
FGF	fibroblast growth factor
GPCR	G-protein coupled receptor
HCl	hydrochloric acid
HE	hematoxylin and eosin
HSC	hematopoietic stem cells
KO	knock-out
mRNA	messenger RNA
NaCl	sodium chloride

NAFLD	non-alcoholic fatty liver disease
NaOH	sodium hydroxide
NH_4OH	ammonium hydroxide
PAM	protospacer-adjacent motif
PBS	phosphate-buffered saline
PCR	polymerase chain reaction
PFA	paraformaldehyde
RNA	ribonucleic acid
RT-qPCR	real-time quantitative polymerase chain reaction
sgRNA	single-guide RNA
STM	septum transversum mesenchyme
TGN	trans-Golgi network
TMED	transmembrane emp24 domain
qPCR	quantitative PCR

CHAPTER 1

Background

1.1 Introduction

Protein trafficking is an important cellular function which traffics nascent proteins destined to be secreted or membrane-bound in their mature functional configuration. It is crucial during embryonic development where dynamic cellular processes require an intricate network of communication between different cell-types. Communication between cell-types can occur via secreted signaling molecules and cell surface receptors to coordinate cellular proliferation and differentiation. For example, Wnt/Frizzled signaling, involving the secreted Wnt ligand interacting with Frizzled receptor on target cells, is highly implicated in the patterning of the body axis as well as morphogenesis in vertebrates (Port and Basler, 2010; Sokol, 2015). In this case, protein trafficking is needed to secrete Wnt from Wnt-producing cells and also to express the Frizzled receptor at the plasma membrane of cells to respond to Wnt ligand.

Additionally, mutations in components of the secretory pathway can lead to congenital diseases and embryonic defects. For example, mutation in the Sec24b leads to craniorachischisis (defect in neural tube closure observed in neonates) (Merte et al., 2010), mutation in Sec24c is embryonic lethal by embryonic day (E) 7 in mouse (Adams et al., 2014), and Sec24d mutation is associated with craniofacial malformations and ossification defects (Garbes et al., 2015). Thus studying the role of specific proteins involved in the secretory pathway will lead to a deeper understanding of embryonic development which can lead to understanding human syndromes arising from deregulated embryonic development.

1.2 Protein trafficking and vesicle transport

Proteins that do not reside in the cytosol (secreted (luminal) and membrane-bound proteins) require protein trafficking in order to be localized to the appropriate sub-cellular

compartment. These proteins are first assembled from amino acids via cytosolic ribosomes using messenger RNA (mRNA) as templates. These nascent proteins contain a signal sequence which is recognized and transported co-translationally or post-translationally by the signal recognition particle (SRP) and the signal receptor (SR) into the lumen of the endoplasmic reticulum (ER) through the protein channel Sec61 (Kalies et al., 2008; Rapoport et al., 1996; Segev, 2009; Stirling et al., 1992; Walter and Johnson, 1994).

Proteins translocated into the ER lumen undergo folding to acquire its mature conformation through the assistance of chaperones (ex. heat-shock proteins (HSPs)) and protein modifications (ex. glycosylation). Misfolded proteins either remain in the ER until properly folded or may undergo ER-associated degradation (ERAD) in order to minimize ER-stress (Piper and Bryant, 2009). Once properly folded, proteins are then shuttled to the ER Golgi intermediate compartment (ERGIC) and then to the cis-Golgi network (CGN) where further protein modifications may occur in order to produce mature proteins. The mature protein is sorted from the trans-Golgi network (TGN) to endosomes, the plasma membrane or other organelles as necessary (Piper and Bryant, 2009).

Transport between compartments of the secretory pathway is mediated by three types of protein-coated vesicles, the type used depends on which organelle compartment is generating these vesicles: coat protein (COP) II coated vesicles mediate ER-to-ERGIC transport, COPI mediates inter-Golgi membrane transport and recycling of proteins from the Golgi/ERGIC back to the ER, and clathrin mediates vesicular transport between the TGN and the plasma membrane (Mancias and Goldberg, 2008; Segev, 2009; Stagg et al., 2006). The formation of vesicles is in part associated with small GTPases such as Arf1 and Sar1 which help recruit coat proteins to the lipid bi-layer (Long et al., 2010; Spang, 2002; Yorimitsu et al., 2014).

Cargo receptors are involved in promoting the formation of transport vesicles, however, they are more crucially involved in recruiting specific properly-folded cargo proteins into the forming vesicles (Piper and Bryant, 2009). Thus, cargo receptors are crucial for regulating the expression of membrane-bound and secreted proteins of a cell.

1.3 TMED Proteins

The transmembrane emp24 domain-containing family (TMED) contains a set of type I single-pass transmembrane proteins known to be involved in the secretory pathway as cargo receptors. TMED proteins are further categorized into subfamilies α, β, γ, and δ as a function of sequence similarity (Dominguez et al., 1998; Strating et al., 2009). Depending on the type of organism, different numbers of each subfamily can be found: vertebrates have 10 members (3 α, 5 γ, 1 β and 1 δ). TMED proteins share the following common structural domains: a signal sequence, a globular golgi-dynamics (GOLD) domain predicted to contain a disulfide bridge (Nagae et al., 2016), a coiled-coil domain, a transmembrane domain, and a short cytoplasmic tail. The signal sequence is required for the translocation of TMED proteins into the ER membrane during translation (Walter and Johnson, 1994); the GOLD domain is mainly associated with the interaction with cargos during vesicular transport. The coiled-coil domain is primarily involved in the interaction between TMED family members during oligomerization and the short cytoplasmic tail contains binding motifs crucial for mediating binding with COPI and/or COPII coat proteins during vesicular transport.

It was previously shown that TMED proteins from different subfamilies can form hetero-dimeric and hetero-tetrameric complexes (Jenne et al., 2002). This was further supported by observations that altering the expression levels of a single TMED member can affect the

expression levels of TMED proteins in other subfamilies (Buechling et al., 2011; Hou et al., 2017; Jerome-Majewska et al., 2010; Theiler et al., 2014). Crystal structures of the GOLD domains of TMED10 and TMED2 revealed that these two TMED proteins can interact via their GOLD domains (Nagae et al., 2016). TMED proteins may function in complexes for cargo recognition and/or may be a method for facilitating their recovery from the Golgi back to the ER via COPI-coated vesicles.

1.4 TMED2 Interactions and Implications

TMED2 was demonstrated to interact with TMED10 in COPI vesicles and Golgi compartments of the cell in association with SM18 (a sphingomyelin species) (Contreras et al., 2012; Gommel et al., 1999). In further support for TMED2's involvement in COPI vesicle formation, TMED2 was found to interact with ARF1 and ARF GTPase activating protein and regulate the formation of COPI vesicles (Majoul et al., 2001). In addition, TMED2 was also found to bind to Sec23 (COPII coat protein) and that the interaction depended on a diphenylalanine (FF) motif (Dominguez et al., 1998). The association of TMED2 with COPI vesicle formation may allow it to function as a quality control checkpoint, recognizing and transporting misfolded proteins back to the ER while its association with COPII vesicles allows it to function as a cargo receptor. In summary, TMED2 is largely sequestered to the early secretory pathway and is involved in vesicular transport between the ER and Golgi apparatus.

TMED2 is understood to be a cargo receptor which recognizes and assists in the transport of cargo proteins to the Golgi apparatus by interacting with cargo receptors via its luminal domain. However, the link between TMED2's target protein cargoes and its physiological role during ontogeny remains unclear. Several studies have identified cargoes in invertebrate

organisms. In yeast, TMED2 was identified to be important in the secretion of invertase and Gas1p to the periplasmic space (Stirling et al., 1992). It was later demonstrated that TMED2 may complex with TMED10 in yeast to bind to Gas1p and mediate its transport from the ER. This suggests that TMED2 may be involved in the trafficking of glycosylphosphatidylinositol (GPI)-anchored proteins. *Lin-12* or *Glp-1* (components of the *C. elegans* Notch signalling pathway) mutation in *C. elegans* leads to defects in cell fate decisions which was exacerbated when *Sel-9* (TMED2 homologue) was also mutated (Wen and Greenwald, 1999); the authors postulated that Sel-9 protein may act as a quality control checkpoint recognizing and preventing misfolded Lin-12 and Glp-1 protein from being trafficked to the cell surface. TMED2 has also been implicated in the secretion of Wnt proteins in *Drosophila*. CHOp24/Emp24 (*Drosophila* homolog of TMED2) interacts with wingless (Wg) and knockdown of Emp24 resulted in the accumulation of Wg in the ER (Buechling et al., 2011; Li et al., 2015; Port et al., 2011). Additionally, Emp24 knockdown generated a mild form of the wing margin defect observed in Wg-mutants (Buechling et al., 2011; Port et al., 2011). All in all, these studies support that TMED2 functions as a cargo receptor regulating the trafficking of specific cargos, and that these interactions are involved in embryonic development.

In vertebrate systems, several TMED2 cargo targets have been identified. The immature form of Calcium sensing receptor (CaSR) (a G-protein coupled receptor) was discovered to interact with TMED2 which allows its transport from the ER to the Golgi-apparatus (Stepanchick and Breitwieser, 2010). The glucagon receptor (GCGR) was also identified to interact with TMED2 in its liganded (glucagon-bound) state but not the un-liganded state; with TMED10 interacting indirectly with liganded GCGR via TMED2 (Junfeng et al., 2015). In the same study, it was revealed that overexpression of TMED2 in Chinese hamster ovary (CHO)

cells led to increased glucagon-induced glucose production but not basal glucose levels. Interestingly, TMED2 was also implicated in the receptor resensitization pathway of a thrombin receptor called PAR-2, a GPCR, whereby TMED2 interacts and maintains PAR-2 at the TGN only dissociating from this protein once plasma membrane stocks of PAR-2 are activated and endocytosed (Luo et al., 2007). In addition to PAR-2, the authors later demonstrated that other GPCRs also interacted with TMED2: PAR-1, $P2Y_1R$, $P2Y_2R$, $P2Y_4R$, $P2Y_{11}R$ and MOR1B (Luo et al., 2011). This raises the possibility that TMED2 may be an important regulator of GPCR trafficking.

1.5 Liver Organogenesis

The liver proper is formed from derivatives of the endoderm as well as mesoderm. Parenchymal components of the liver are derived from hepatoblasts (bi-potential hepatic progenitor) in the endoderm, whereas the stromal component and vasculature are derived from the mesoderm. Murine gestation lasts about 20 days, the embryonic age is denoted as embryonic days (E) past the discovery of a vaginal plug produced during coitus. Morphologically, a liver diverticulum consisting of hepatoblasts is induced at the caudal ventral foregut endoderm at embryonic day 9.0 (E9.0), the diverticulum develops into a liver bud at E9.5 as hepatoblasts delaminate and infiltrate into the surround septum transversum mesenchyme (STM) and the liver bud subsequently expands in size until four weeks of age postnatal (Fig 1) (Harvard Stem Cell, 2008).

Hepatoblast cells in the liver diverticulum are induced by fibroblast growth factor (FGF) 1 and FGF2 signaling from the cardiac mesoderm and bone morphogenic protein (BMP) signaling from the STM (Jung et al., 1999; Rossi et al., 2001). Delamination of hepatoblasts from

the foregut epithelium requires the expression of transcription factors *Prox1, Gata-4, Gata-6* and *Hhex* (Bort et al., 2006; Sosa-Pineda et al., 2000; Watt et al., 2007; Zhao et al., 2005). Additionally, this process also requires hepatoblast interaction with the surrounding blood vessels associated with *Vegfr-2* expression and interaction with the extra-cellular matrix via *β1*-integrin (Fässler and Meyer, 1995; Matsumoto, 2001).

During this period of liver bud expansion hepatoblasts are differentiating into hepatocytes and cholangiocytes, biliary ducts are forming, the liver is vascularizing and the hepatic lobules (functional units of the liver) are forming (Fig 1). The expansion of the liver requires hepatocyte growth factor (HGF) expression (Schmidt et al., 1995) and Wnt/*β*-catenin signaling in hepatoblasts and hepatocytes (Apte et al., 2007; Tan et al., 2008). Furthermore, it was observed that STM-specific knockout of *Gata-4* is embryonic lethal by E13.5, and prior to death the liver was hypoplastic, secondary to increased apoptosis (Delgado et al., 2014).

During mid-to-late gestation (E9.5 to E15.5), the liver is the first major site of definitive hematopoiesis; hematopoietic progenitors infiltrate the developing liver and the organ acts as a niche for proliferation and differentiation (see Section 1.6).

1.6 Prenatal liver and its contributions to embryonic hematopoiesis

During embryonic development, the liver is crucial for definitive hematopoiesis – the generation of mature hematopoietic cells which will populate the adult hematopoietic system. The role of the liver consists of providing the proper environment for the expansion and differentiation of HSC generated *de novo* from the aorta-gonad-mesonephros (Godin et al., 1999). The micro-environment of the embryonic liver involved in hematopoiesis is currently being investigated, but liver stromal cells are speculated to be involved (Sakane et al., 2004).

Different hematopoietic precursor cells peak at certain ages during the liver's involvement in embryonic hematopoiesis (Fig 1): T cell precursors expand between E11-12 and exit by E13 (Ema et al., 1998). Additionally, liver-resident macrophages are involved in the maturation of erythrocytes by contributing to the enucleation of nucleated erythrocytes; nucleated erythrocytes infiltrate the liver as early as E11.5 and enucleation occurs between E14.5-E16.5 (Crawford et al., 2010; Isern et al., 2008).

Within the hematopoietic cell lineage, there are key transcription factors involved in regulating lineage development and differentiation (Fig 2 & Table 4): for example, C/EBPε, Gata-1, Jun, PU.1 and Gata-3. Complete knock-out of *Pu.1* results in mice with no mature neutrophils, B cells, T cells and macrophages at birth, however neutrophils and T-cells re-appear at postnatal day 10 (McKercher et al., 1996). C/EBPε cooperates with PU.1 to mediate neutrophil maturation and differentiation by promoting nuclear segmentation (Malu et al., 2016). Gata-1 null mice are embryonic lethal as a result of halted erythrocyte development (Fujiwara et al., 1996). Jun was found to enhance the expression of macrophage colony stimulating factor receptor (important in monocyte survival and differentiation) via interaction with PU.1 (Behre et al., 1999). Additionally, Jun null mutation was found to be embryonic lethal and exhibited impaired hepatogenesis and erythropoiesis (Hilberg et al., 1993). Gata-3 null embryonic stem cells fail to develop into T cells (Ting et al., 1996). Since many genes involved in embryonic development results in complex embryonic defects or embryonic lethality when mutated, an alternative to complete KO is required to elucidate the function of genes with better spatial-temporal precision.

1.7 Cre/loxP Recombination System

Heterozygous and homozygous genetic mutants are useful in determining the requirement of a gene in an organism. However, since the gene is completely removed from all cell lineages at all time points in the organism, precision is lost during the analysis of gene function limiting our understanding of its temporal-spatial requirements during ontogeny. Mutations of broadly expressed genes may be embryonic lethal, precluding the analysis of the function of this gene at a later time point in development. Multiple lineages of cells may require the same gene to function and complete KOs of a single gene do not allow researchers to segregate the functions of the gene in these different lineages. As such, the development of conditional gene mutation using Cre/loxP technology to ablate genes in a tissue-specific manner has become a powerful tool for the study of gene function.

The Cre/loxP recombination system was identified in bacteriophage P1. This system demonstrated the ability for site-specific recombination using only the Cre recombinase enzyme (Cre) and two loxP sites in a genomic region (Abremski et al., 1983; Sternberg and Hamilton, 1981). Cre/loxP technology allows for the deletion of a gene of interest in specific-tissues first demonstrated by Kühn et al (Kuhn et al., 1995). Since then, mouse lines expressing a loxP site flanked (floxed, abbreviated as 'fl') gene are often mated to transgenic mice expressing Cre under a tissue-specific promoter to uncover its requirement in the Cre-expressing tissue (Akira, 2000; Brehm et al., 2007; Delgado et al., 2014). For example, conditionally inactivating *Gata-4* in the STM using Cre/loxP technology revealed a role for STM *Gata-4* expression in hepatic proliferation (Delgado et al., 2014). Furthermore, a mouse strain carrying the ROSA26 Cre reporter was developed to enable the tracking of Cre activity in Cre/loxP conditional KO experiments (Soriano, 1999). The ROSA26 transgenic allele carries a lacZ reporter with a

premature stop codon flanked by loxP sites. Upon Cre expression, the stop codon is removed and lacZ is expressed allowing researchers to track in which morphological structures the gene of interest was removed.

1.8 CRISPR/Cas9 endonuclease and homology-directed repair

The clustered regularly interspaced short palindromic repeats (CRISPR) system was discovered to be an adaptive immune response in prokaryotes which induces DNA double-stranded breaks (DSB) to defend against invading phage DNA (Barrangou et al., 2007; Sapranauskas et al., 2011). There are several varieties of CRISPR systems; in general these require small RNA particles which are homologous to the target sequence to recruit the CRISPR-associated (Cas) proteins to the target loci in order to produce DSB (Makarova et al., 2011). In type II systems, it was discovered that Cas9 protein interact with two RNA molecules to form a ribonucleic complex in order to recognize its target DNA sequence and produce a DSB: CRISPR-associated RNA (crRNA) and trans-activating crRNA (tracrRNA) (Jinek et al., 2012). Interestingly, the authors also observed that crRNA and tracrRNA could be replaced by a crRNA:tracrRNA chimera referred to as a single guide RNA (sgRNA) to induce DSB. This demonstrated the ease and versatility of the CRISPR/Cas9 system as a tool for studying genes via targeted-genome editing (Jinek et al., 2012). The crystal structure of the interaction between these components has been elucidated (Anders et al., 2014). A requirement of the target sequence is that there must be a proto-spacer adjacent motif (PAM) of nucleic acid sequence - NGG at the 3' end of the sgRNA sequence (Jinek et al., 2012; Mojica et al., 2009). Recently, Shibata et al. visualized the action of CRISPR/Cas9 induced DSB using high-speed atomic force microscopy (Shibata et al., 2017).

The ability for CRISPR/Cas9 to induce site-specific DSB allows researchers to generate gene KO by targeting protein coding sequences of the gene of interest using specific sgRNA design and Cas9 mRNA/protein. The CRISPR reagents are often introduced by microinjection (Wang et al., 2013; Yang et al., 2013). Furthermore, because the specificity of Cas9 targeting depends only on sgRNA homology to the target sequence, simultaneous use of multiple sgRNAs allows for the multiplex targeting of several genes of interest (Wang et al., 2013). Alternative to microinjections, it has been suggested that electroporation is a better method for introducing CRISPR/Cas9 reagents into zygotes and that this leads to better efficiency of CRISPR/Cas9-mediated edits (Chen et al., 2016). In addition, researchers can insert stretches of sequence by providing a repair template; using this strategy, fluorescent tags and loxP sites have been successfully inserted in target genes (Paix et al., 2017; Yang et al., 2013). However, founder mouse populations from CRISPR/Cas9 microinjection experiments using zygotes have yielded mosaic edits (Yen et al., 2014) and yields in homology-directed knock-in experiments have been low (Wang et al., 2015).

1.9 Rationale

Tmed2 null mutants are embryonic lethal by E11.5 as a result of the inability to properly form the placenta (Jerome-Majewska et al., 2010). This precludes the analysis of *Tmed2* null embryos past E11.5, during which organogenesis is occurring raising the necessity for an alternative approach to investigating phenotypes that may arise from TMED2 removal during organogenesis. Since the Cre/loxP system enables the excision of stretches of DNA (ex. exons) in a temporal-specific and/or tissue-specific manner, a useful strategy for studying the role of *Tmed2* would be to generate mice with a floxed (fl) conditional KO allele of the *Tmed2* locus (i.e. $Tmed2^{fl/fl}$). Breeding these mice with *Cre*-expressing transgenic mice under a gene

promoter that is expressed tissue or temporal-specifically would allow for the identification of phenotypes arising from lack of TMED2 in a more precise manner.

Prior to embryonic death, *Tmed2* null mutants present with severe developmental delay which suggests that TMED2 is required prior to the embryo's dependence on maternal-derived nutrients via placental circulation, however, in what developmental processes it participates in remains to be addressed. *Tmed2* mRNA was also expressed in many structures during embryonic development, namely the liver diverticulum at E9.5 (Jerome-Majewska et al., 2010) and TMED2 protein was found to be expressed in the liver at E17.5 and P5 (unpublished data); time points in which the liver is still developing and maturing into its adult form. Since *Tmed2* is expressed in the embryonic liver during development, and the liver functions as the primary site of definitive hematopoiesis during embryonic development, we hypothesize that *Tmed2* is required for the development of the liver. In this study we've focused primarily on identifying a role for TMED2 in liver hematopoiesis.

1.10 Objectives

To address the established hypothesis, the following aims were determined:

1. Investigate whether liver hematopoiesis is altered in *Tmed2*$^{99J/+}$ mice.
2. Generate *Tmed2*$^{fl/fl}$ mice and mate these to *Alb-Cre* transgenic mice to remove TMED2 liver-specifically.

CHAPTER 2

Materials and Methods

2.1 Mice

All work concerning mice was performed according to guidelines of the Canadian Council on Animal Care (CCAC) and approved by the Animal Care Committee of the Research Institute of the McGill University Health Center. All wild-type animals used to generate embryos or for expanding mutant mouse lines were purchased from The Jackson Laboratory. *Tmed2*$^{99J/+}$ mice used for analysis of the liver were previously generated by our lab.

Embryo and liver collection

For embryo collection, the day which a vaginal plug was observed was considered as embryonic day 0.5 (E0.5). For liver collection, the date of birth was considered to be postnatal day 0 (P0). Embryos from *Tmed2*$^{99J/+}$ x wild-type C3H mice crosses were harvested at E14.5 and E17.5. Livers were also collected at P5.

The genetic backgrounds of embryos obtained from micro-injections were:

- CD1 (Round 1)
- CD1:FvB (Rounds 2 – 4)
- C3H:C57Bl/6 (Rounds 5 and 6)

2.2 Genotyping

For embryos, the yolk sac was collected during harvest for genotyping. For mice, tail clippings were collected for genotyping.

Crude genomic DNA was extracted from yolk sacs and tail clippings using the alkaline lysis method: the tissues were incubated in 75ul alkaline lysis reagent (25mM NaOH, 0.2mM

EDTA in ddH_2O) at 95^oC for 30 min, then cooled on ice and neutralized by adding 75ul neutralizing buffer (40mM Tris-HCl, pH5.0 in ddH_2O). The neutralized DNA preps of yolk sacs were used directly as DNA template for PCR genotyping. For tail clippings, the neutralized DNA preps were diluted by adding 300ul ddH_2O before PCR genotyping, as DNA concentration is higher from tail clippings compared to yolk sacs.

Genotyping of mice with the 99J mutation

The 99J mutation is a point mutation generated on the C57/Bl6 genetic background and maintained on a C3H genetic background. As such, mice and embryos generated from the 99J line were genotyped by PCR using primers designed to amplify D5MIT95 and D5MIT213 as previously described (Hou et al., 2017; Jerome-Majewska et al., 2010).

Genotyping of mice from CRISPR/Cas9 micro-injections

Using Primer3 (Koressaar and Remm, 2007; Untergasser et al., 2012), primers were designed to amplify the region flanking loxP insertion sites in the *Tmed2* locus in intron 1 or intron 2.

List of intron 1 primers:

Tmed2-F2: 5'- AGGTCGCTGGATCTCTGAAT -3'

Tmed2-R2: 5'- GAGCCTCCCCAATGTCAATG -3'

Tmed2-F5: 5'- GAGGCCATGTGGAGAGTTGT -3'

Tmed2-R5: 5'- TAGCAGCATCCTCACAGGAA -3'

List of intron 2 primers:

Tmed2-F4: 5'- TCTATAAAGGAGACCGGGAGT -3'

Tmed2-R4: 5'- AAAACCACTCTCATGCCAGC -3'

Tmed2-F6: 5'- ATTTTGGTTGTGCCTTCTGG -3'

Tmed2-R6: 5'- GGATGCTGTCACACAAAAGC -3'

Primer pairs were used in the following configurations: F2R2, F5R5 and F5R2 for intron 1 and F4R4 and F6R6 for intron 2. For all primer pairs, the PCR cycling condition used was: 95^{o}C initial denaturation for 3 min, 38 cycles of amplification (95^{o}C for 30 secs, 56^{o}C for 50 secs, then 72^{o}C for 1 min), and a final elongation step at 72^{o}C for 5 min.

Restriction digestion enzymes (EcoRI, EcoRV and XbaI) were purchased from New England BioLabs. 5ul of PCR product was restriction digested in a 10ul final volume according to manufacturer's recommendations. The restriction digestion reaction was performed at 37^{o}C for 1 hour.

The expected sizes for PCR products using the designed primers and restriction digestion products are as follows (Note: the expected loxP amplicon sizes and restriction digestion enzyme depend on which repair template was used):

Tmed2 Intron 1

Tmed2-F2R2:

wt = 591bp

Repair Template 1 or 3: loxP = 631bp; loxP + EcoRI = 308bp and 323bp

Repair Template 4: loxP = 608bp; loxP + EcoRI = 298bp and 310bp

Tmed2-F5R2:

wt = 441bp

Repair Template 5: loxP = 458bp; loxP + XbaI = 148bp and 310bp

Tmed2-F5R5:

wt = 228bp

Repair Template 1 or 3: loxP = 268bp; loxP + EcoRI = 115bp and 153bp

Tmed2 Intron 2

Tmed2-F4R4:

wt = 634bp; wt + EcoRV = 56bp and 578 bp

Repair Template 2 or 3: loxP = 674bp; loxP + EcoRV = 56bp, 215bp and 403bp

Repair Template 5: loxP = 651bp; loxP + XbaI = 227bp and 424bp

Tmed2-F6R6:

wt = 230bp

Repair Template 2 or 3: loxP = 270bp; loxP + EcoRV = 93bp and 177bp

Putative loxP site insertions and other mutations of interest were confirmed by Sanger sequencing at the McGill University and Genome Quebec Innovation Centre.

2.3 CRISPR/Cas9-mediated insertion of loxP sites flanking *Tmed2* exon 2

Microinjections were performed either at the Centre de recherche du CHUM (microinjection rounds 1- 4) or at the McGill Goodman Cancer Research Center (microinjection rounds 5 and 6).

CRISPR sgRNA and DNA repair templates were designed based on mouse genome assembly GRCm38/mm10 (UCSC Genome Browser).

sgRNA design and synthesis

sgRNAs were designed to target intron 1 and intron 2 of *Tmed2* using the CRISPR Design tool from the Zhang lab (Hsu et al., 2013). The guides were then screened for nucleotides favorable for deletion events induced by CRISPR/Cas9 (Xu et al., 2015).

Synthesis of sgRNAs was performed using the GeneArt™ Precision gRNA Synthesis Kit (ThermoFisher Scientific) according to the manufacturer's protocol: Briefly, a sgRNA DNA template for each sgRNA was assembled by PCR reaction using primers containing the corresponding spacer sequence, the sgRNA DNA templates were then *in vitro* transcribed into RNA using an NTP mix, TranscriptAid™ Enzyme Mix and reaction buffer (Thermo Fischer Scientific) incubating at 37°C for 3 hours, and the transcribed sgRNA was purified using the GeneJET™ RNA Purification Micro Columns (ThermoFisher Scientific). PCR-assembled sgRNA DNA templates were verified for proper assembly on 4% agarose gels before use for *in vitro* transcription. Purified sgRNAs were verified by Urea PAGE (Summer et al., 2009) on a 12.5% polyacrylamide gel treated with urea to confirm the presence and purity of the synthesized sgRNAs before use in micro-injection experiments.

DNA Repair Template Design

DNA repair templates were designed to target the insertion of a restriction digestion site and loxP site at the *Tmed2* intron 1 and intron 2 sgRNA:Cas9 target DNA sites - 3bps upstream of the PAM sequence. Repair templates were ordered as PAGE-purified Ultramer® DNA Oligo (Integrated DNA Technologies) and re-suspended in ddH_2O. A total of 5 different repair templates were used (see Figure 3 & 8):

- Repair Template 1 (Fig 3): 140nt single-stranded oligonucleotide targeting *Tmed2* intron 1 containing EcoRI and loxP sequence flanked by 50nt of sequence homologous to intron 1.
- Repair Template 2 (Fig 3): 140nt single-stranded oligonucleotide targeting *Tmed2* intron 2 containing EcoRV and loxP sequence flanked by 50nt of sequence homologous to intron 2.
- Repair Template 3 (Fig 3): 723nt double-stranded gene fragment containing (from 5' to 3') 50nt sequence homologous to *Tmed2* intron 1, EcoRI and loxP sequence, intron 1 homologous sequence, *Tmed2* exon 2 homologous sequence, homologous sequence to *Tmed2* intron 2, EcoRV and loxP sequence, and 50bp sequence homologous to intron 2.
- Repair Template 4 (Fig 8): 198nt single-stranded oligonucleotide targeting *Tmed2* intron 1 containing EcoRI and loxP sequence flanked by 5' 64nt sequence homologous to intron 1, and 3' 94nt homologous to intron 1 with one sgRNA binding site deleted and the other sgRNA binding site containing 4 mutated bases near or in the PAM sequence.
- Repair Template 5 (Fig 8): 200nt single-stranded oligonucleotide targeting *Tmed2* intron 2 containing loxP and XbaI sequence flanked by 5' 134nt sequence homologous to intron 2 with one sgRNA binding site deleted and the other site containing 4 mutated bases near or in the PAM sequence and a 3' 26nt sequence homologous to intron 2.

2.4 T7 endonuclease assay

The T7 endonuclease assay was performed on PCR products obtained from blastocyst DNA extracted using a previously established protocol (Takayuki et al., 2014) and tail DNA obtained as described in Section 2.2.

A 20ul reaction was set up according to manufacturer's protocol for T7 endonuclease I (New England Biolabs; NEB): 10ul PCR product, 2ul 10X NEBuffer 2, and 8ul ddH_2O. The reaction mixture was incubated in a thermocycler to denature and re-nature the PCR product: 95°C for 5 min, ramp of -2°C/s to 85°C and hold for 5 sec, ramp of -0.1°C/s to 25°C and hold for 5 sec and infinite hold at 4°C. Next, 0.75ul of T7 endonuclease I (NEB) was added to the reaction mixture and incubated at 37°C for 30 min. The T7-treated samples were analyzed on a 2% agarose gel.

2.5 Collection, sectioning and staining of liver samples

Liver tissue collection and processing for histology

Mice were anesthetized using isofluorane and then euthanized by CO_2 asphyxiation. A portion of the left liver lobes were harvested and fixed overnight in 4% PFA at 4°C. Next, the livers were processed in the following solutions for 30 min each at 4°C: PBS (twice), 0.25M sucrose/0.2M glycine in PBS, 100% EtOH:1.5% NaCl (1:1) and 70% EtOH (twice). The livers were then dehydrated in the following solutions for 30 min each at room temperature: 85% EtOH, 95% EtOH and 100% EtOH (twice). Clearing was performed in the following solutions for 30 min each at room temperature: EtOH:xylene (1:1), xylene (twice), and xylene:paraffin (60:40). Lastly, the livers were washed four times in paraffin at 60°C for 30 min each and embedded in paraffin blocks using the Leica EG1160 Embedding Center (Leica Biosystems).

Livers were sectioned at 5um thickness on a Leica RM 2155 microtome (Leica Biosystems) and five serial sections were mounted on each glass slide.

HE Staining

Liver sections were de-paraffinated with two 10 min xylene washes. Rehydration was then performed in the following solutions for 5 min each: 100% EtOH (twice), 95% EtOH, 70% EtOH, ddH_2O. The sections were stained in Harris Hematoxylin Solution (Sigma-Aldrich) for ~2 min (staining was monitored until desired color was obtained), followed by a differentiation step of 5 dips in acid water (12 drops of HCl in 200ml ddH_2O) and 10 min in running tap water, and lastly the bluing step was performed by 5 dips in ammonia water (12 drops NH_4OH in 200ml of ddH_2O) followed by 10 min rinse in running tap water. For eosin staining, the hematoxylin-stained sections were washed with 95% EtOH for 5 min, and then stained by 5 dips in Eosin Y Solution (Sigma-Aldrich). Excess eosin staining was removed with 3 dips in 95% EtOH and 2 dips in 100% EtOH. Slides were then rinsed in two 5 min washes of xylene and coverslipped using Permount® (Fisher Scientific).

2.6 Peripheral blood collection and complete blood count analysis

Mice were sacrificed by isofluorane-induced anesthesia followed by CO_2 asphyxiation. The abdominal and thoracic cavities were then opened to expose the heart using forceps and dissecting scissors. Peripheral blood was harvested by cardiac puncture and immediately collected in EDTA-treated collection vials.

Complete blood count analysis was performed at McGill's Comparative Medicine and Animal Resource Center (CMARC) Diagnostics Laboratory.

2.7 Tail bleeding assay

Weights of mice were obtained prior to the procedure. They were then anesthetized using isofluorane. Animals were placed in a prone position on a raised platform and maintained under anesthesia by isofluorane fed through an anesthesia mask for the duration of the experiment. The

tip of the tail was then clipped and placed in PBS (pH 7.4) pre-warmed to 37^{o}C. A timer was started at the time of tail clipping and the bleeding (visualized as a stream of blood in the PBS) was monitored for 4 min: the points in time (relative to the time of tail clipping) at which bleeding started and stopped were noted. Average bleeding duration and number of re-bleeds were compared using a t-test – re-bleed was defined as the number of times within 4 min that the bleeding would start and stop after the initial bleeding.

2.8 RT-qPCR primer design, cDNA synthesis and qPCR

RT-qPCR was performed on RNA from whole livers collected at E14.5. Embryos were dissected in DEPC treated PBS; livers were collected in Eppendorf tubes and snap frozen on dry ice.

Primer Design

Primers for RT-qPCR were designed using Primer-BLAST (National Library of Medicine). The tool was configured to search for primer pairs which generate a PCR product size below 400bp and which at least one primer of the pair must span an exon-exon junction to detect mRNA. See Table 1 for the list of primers used in RT-qPCR experiments.

RNA Extraction

mRNA was extracted using the TRIzol method. Each liver was homogenized in 800ul of TRIzol® Reagent (Life Technologies) using a sonicator and let rest at room-temperature for 5 min. 160ul of chloroform was then added into the tube and mixed by inverting followed by a 3 min incubation at room-temperature. Then the mixture was centrifuged at 12,000rcf (relative centrifugal field) for 15 min at 4^{o}C. The aqueous phase (uppermost) was transferred to a fresh

tube and 400ul of Isopropyl alcohol was added; solution was mixed by inverting. The mixture was incubated for 10 min at room-temperature and then centrifuged at 12,000rcf for 10 min at 4°C; the supernatant was discarded. The RNA pellet was washed with 800ul of 75% EtOH (prepared with DEPC-treated ddH_2O) by inverting the tube. The RNA was re-pelleted in a centrifuge at 12,000rcf for 5 min at 4°C. Using a P1000 pipette, as much EtOH as possible was removed without disturbing the pellet. The RNA was re-pelleted at 13,000rcf for 5 min at 4°C, and the remaining EtOH was removed using a P200 pipette. The RNA pellet was let dry for 10 seconds with the eppendorf lid opened. The pellet was then re-suspended in 20ul of RNase free water and heated at 60°C for 10 min, then 5 min at room-temperature and stored at -80°C.

Prior to storage, the RNA concentration of each sample was measured using the NanoDrop™ 2000 Spectrophotometer (Thermo Fisher Scientific).

DNAse I Treatment

Extracted RNA was treated with DNase I (NEB): 2ul of 10X DNase I reaction buffer and 2ul DNaseI was added to 10ug of RNA and the mixture was filled with DEPC-treated ddH_2O to a final volume of 20ul. The reaction mixture was incubated at 37°C for 10 min. 0.2ul of 0.5M EDTA was added to the reaction and incubated at 75°C for 10 min to inactive DNase I.

Reverse Transcription

Reverse transcription was performed using the iScript™ Reverse Transcription Supermix for RT-qPCR (BioRad) according to manufacturer's protocol. A 10ul reaction volume containing 2ul iScript RT Supermix, 2ul DNAseI-treated RNA and 16ul nuclease-free water was set up. The reverse transcription reaction was performed in a thermocycler: 5 min at 25°C, 20 min at 46°C and 1 min at 95°C. The cDNA was diluted by adding 90ul of ddH_2O before use for qPCR.

qPCR

The qPCR reaction was performed in a light cycler LC480 (Roche) using SsoAdvanced™ Universal SYBR® Green Supermix. The final reaction volume was 10ul, containing: 5ul SYBR Green Supermix (2X), 0.7ul 10uM primer mix (10uM forward and 10uM reverse primer), 3ul of cDNA and 1.3ul of nuclease-free H_2O. The cycling parameters included the following: 95°C for 5 min, 40 cycles of amplification (95°C for 10s, 60°C for 30s).

Each experiment was performed in duplicate. For analysis, the Ct values were exported as tab-delimited text files. Analysis was performed in Microsoft Excel: the average Ct value (avgCt) between technical replicates was calculated, the avgCt was substracted from the lowest avgCt ($avgCt_{min}$) for each sample within the same gene ($avgCt_{min}$ - avgCt), and for each sample a fold change was obtained by calculating $2^{(avgCtmin - avgCt)}$. The fold change was normalized to a normalization factor generated using geNorm software (v3.4) (Vandesompele et al., 2002) based on the expression level of *Actb, B2m and Sdha* internal control genes. The average normalized expression level of the target gene between wild-type and $Tmed2^{99J/+}$ animals were compared using a standard t-test.

2.9 Statistical Analysis

Statistical analyses were either performed using GraphPad Prism or Microsoft Excel 2007. For cell proportion analysis, two-factor ANOVA was performed with Sidak's multiple comparisons correction applied when an interaction between genotype and sex was significant. Mean bleeding times in the tail bleeding assay were comparing using t-tests. Average cell counts from the complete blood count experiment were compared using a Mann-Whitney U test. For all statistical analyses, a p-value ≤ 0.05 was considered significant.

CHAPTER 3

Results

3.1 Homology directed insertion of loxP sites flanking *Tmed2* exon 2

A conditional knock-out (cKO) of a gene of interest refers to a gene that is only mutated under certain conditions. In the case of a loxP cKO allele, a gene or a segment of a gene is flanked by loxP sites (floxed or fl) and the gene is only mutated (DNA segment between loxP sites are excised) upon expression of Cre recombinase. To produce a *Tmed2*$^{fl/fl}$ cKO allele, we decided to flank *Tmed2* exon 2 with loxP sites (one loxP site in intron 1 and the other in intron 2) since the resulting protein, if it is produced at all, would be missing crucial components and produce a non-functional protein. A CRISPR/Cas9-based homology-directed repair strategy was used since it allows for the targeted induction of double-stranded breaks (DSB) which could be used to insert exogenous sequences by repairing using a DNA repair template.

sgRNAs (Table 2 and Fig 3) were designed using the CRISPR Design tool (Hsu et al., 2013) and two sgRNAs were designed for *Tmed2* intron 1 and intron 2: sgRNA 1 and 2 targets *Tmed2* intron 1 and sgRNA 4 and 5 targets *Tmed2* intron 2. Repair templates (Table 3 & Fig 3) were designed to insert loxP sites in *Tmed2* intron 1 and intron 2 via HDR at the expected cut site of the designed sgRNAs; upon repair, the inserted sequence disrupts the sgRNA binding site which avoids sgRNA-induced cutting after proper insertion events. In addition to the loxP site insertion, restriction digestion sites were also included adjacent to the loxP sequence (EcoRI, intron 1 of repair template 1 and 3; EcoRV, intron 2 of repair template 2 and 3) (Table 3 & Fig 3) in order to facilitate genotyping. Six rounds of microinjections were performed at either CR-CHUM or at the McGill Goodman Cancer Research Center using the sgRNA we designed and synthesized and repair templates we designed and purchased (IDT). We then screened for potential loxP insertion by PCR using primers designed to amplify the expected insertion site in

Tmed2 intron 1 and intron 2 (see Methods) and gel electrophoresis. Results from screening are organized below by genetic background of microinjected mice (see sections 3.2 to 3.4).

3.2 No loxP insertion was recovered from micro-injections using CD1 mice

Only microinjection round 1 used CD1 genetic background mice. Overall, seven mice of the CD1 genetic background were born. For these mice, only the sgRNAs for intron 2 (sgRNA 4 & 5) and the repair template 3 were used (Table 2 & Fig 3). Screening using primer pair F2R2 which amplify the *Tmed2* intron 1 insertion site yielded an insertion event in one mouse (Fig 4, left) indicated by the presence of PCR amplicons above the expected wild-type amplicon of 591bp which resembles the predicted 631bp of a proper EcoRI-LoxP insertion according to the repair template that was used (template 3). However, the PCR product did not digest with EcoRI restriction enzyme according to designed repair template (expected size of 308bp and 323bp) (Fig 4, middle). Screening of the same seven mice for an intron 2 insertion using primer pair F4R4 only yielded PCR products of comparable size to the wild-type control (634bp) for all samples (Fig 4, right). Additionally, restriction digestion using EcoRV on PCR products of primer pair F4R4 revealed a restriction digestion pattern comparable to the expected wild-type allele (56bp (not visible), 578bp) (Fig 4, right).

The presence of an insertion in intron 1 suggests that sgRNA 4 and 5, targeting intron 2, are capable of generating DSBs. As such, for subsequent microinjection experiments, we decided to continue using these sgRNAs. Overall, 1 of 7 CD1 mice carried an insertion event in *Tmed2* intron 1 which did not correspond to a loxP insertion.

3.3 Micro-injection using CD1:FvB genetic background mice did not result in *Tmed2* loxP insertion

Microinjections round 2 thru 4 were performed on mice of mixed CD1:FvB genetic background using sgRNAs 1, 2, 4 and 5 and either repair templates 1 and 2 or repair template 3 (Table 2 & Fig 3). A total of 38 mice were born and screened for *Tmed2* loxP insertions. 4 of these mice (1 male and 3 female) harbored intron 1 events but no intron 2 events – these mice were generated from microinjections with repair templates 1 and 2. Using primer pair F2R2 for PCR genotyping, it was observed that 1 male and 2 female mice carried insertion events of different sizes as demonstrated by the presence of PCR products migrating slower compared to the wild-type control (591bp); only one of the insertion events found in a female mouse was of the expected size for a proper loxP insertion (631bp) (see 'Mouse B' in Fig 5a). The last female mouse carried a deletion event as suggested by the presence of a PCR product located below the 400bp mark (see 'Mouse C' in Fig 5a). No events were observed using primer pair F4R4 to genotype for the targeted intron 2 region (not shown). Restriction digestion using EcoRI and EcoRV on the F2R2 and F4R4 PCR products, respectively, did not reveal any digestion products of the expected sizes, suggesting that loxP insertions did not occur. However, we decided to follow up on Mouse B (insertion at around the loxP amplicon size of 631bp) and Mouse C (~200bp deletion): for Mouse B, we wanted to verify if the insertion corresponds to an intact loxP-insertion with a mutated EcoRI restriction site; for Mouse C, since we did not know where the deletion is located (whether intronic or exonic), we wanted to locate the deletion by sequencing and test if it could lead to abnormal developmental phenotypes since a hypomorphic allele would be of interest to study.

To verify that the insertion of expected size in Mouse B does not correspond to a mutated EcoRI restriction site with an intact loxP site, Mouse B (Fig 5a) was first mated with wild-type

C3H animals to produce G1 offsprings heterozygous for the insertion event. 13 G1 mice were born and screened using primer set F2R2 for the intron 1 insertion. 4 of 13 mice carried the insertion event observed in founder Mouse B; however there were three amplicons (even though these mice are heterozygous, see 'Mouse B3 Fig 5b, left) in all of these except for one male mouse (see 'Mouse B2' Fig 5b, left). Mouse B2 was chosen for sequencing as it resembled more what a loxP insertion would appear as; the PCR product above the wild-type (591bp) corresponding to the insertion was extracted from the agarose gel (QIAGEN Kit), sub-cloned into the pCR^{TM}II-TOPO vector, and transformed and amplified in DH5α transformation competent *E coli* in order to facilitate sequencing of the insertion. Plasmid DNA preparation was sent for Sanger sequencing. The sequenced DNA was aligned to repair template 3 used in this microinjection experiment and revealed an insertion of 20bp of unrecognizable sequence in addition to a 12bp deletion of *Tmed2* intron 1 sequence (net insertion of 8bp) (not shown). Together, this data indicates that the insertion was germline transmittable, but that an intact loxP sequence was not inserted into the *Tmed2* intron 1 locus. However, the presence of an insertion suggests that sgRNAs targeting *Tmed2* intron 1 used in this experiment (sgRNA 1 and 2) can produce DSBs but that it was not repaired via HDR using repair template 1.

Since primer pair F2R2 amplifies both *Tmed2* intron 1 and exon 2 sequence, Mouse C with the approximately 200bp deletion observed in a PCR reaction using primer pair F2R2 (Fig 5a) was followed up on to determine the location of the deletion. Mouse C was mated with wild-type C3H animals to generate G1 offsprings heterozygous for the deletion. Of the 26 animals born from breeding, 13 carried the deletion event (see 'Mouse C2' and 'Mouse C3', Fig 5b, right). The product corresponding to the deletion below 400bp was sent for sequencing for both Mouse C2 and C3 using primers F2 or R2. Aligning the sequencing results with wild-type *Tmed2*

sequence (UCSC Genome Browser: RefSeq NM_019770) revealed a 226bp intron 1-only deletion surrounding the site where sgRNA 1 and 2 are expected to produce a DSB and where the loxP insertion is designed to occur (Fig 6). The 226bp deletion does not correspond to highly conserved *Tmed2* intron 1 sequences and no previous literature suggests it may be important for *Tmed2* expression. However, since these animals were already generated and a 226bp deletion is fairly large, we decided to test if it can affect survival of embryos. Thus Mouse C2 (Fig 5b, right) was mated to heterozygous 99J animals (*Tmed2* null mutant) to generate compound heterozygous embryos and mice to test if this intronic deletion could affect survival since 99J homozygous mutants do not survive past mid-gestation (Jerome-Majewska et al., 2010); if the 226bp deletion affects *Tmed2* we would expect to see a phenotype ranging between survival past weaning observed in $Tmed2^{99J/+}$ and embryonic lethality observed in $Tmed2^{99J/99J}$ (Hou et al., 2017; Jerome-Majewska et al., 2010). 11 embryos from a $Tmed2^{99J/+}$ x $Tmed2^{+/\Delta226}$ were dissected at E14.5 and analyzed under a dissecting microscope; all embryos were morphologically comparable (Fig 7a) and no abnormalities were observed when analyzed blind to genotype. Additionally, 12 mice were born from a $Tmed2^{99J/+}$ x $Tmed2^{+/\Delta226}$ and monitored between P8 and P19; no abnormalities were observed when analyzed blind to genotype (data not shown). All embryos and mice were genotyped for the 226bp deletion (primer pair F2R2) and the 99J mutation; overall, there were 4 $Tmed2^{+/+}$, 5 $Tmed2^{+/\Delta226}$, 8 $Tmed2^{99J/+}$ and 6 $Tmed2^{99J/99J}$. The frequency distribution of genotypes was compared to the expected 1:1:1:1 ratio predicted by Mendelian segregation (corresponding to an expected value of 5.75 for each genotype) using a Chi-squared goodness-of-fit test (two-tailed, 3 degrees of freedom); the results were a $\chi^2 = 1.522$ corresponding to p= 0.6773 (Fig 7b). Thus, it was observed that mice from the four genotypes were present in equal abundance and did not present with any visible morphological anomalies.

We concluded that *Tmed2*$^{99J/\Delta226}$ mutants survive. Overall, we found intron 1 events in 4 of 38 (10.5%) of CD1:FvB mice, however none of these events corresponds to the desired loxP insertion.

Since as of yet, the CD1 and CD1:FvB animals generated low frequencies of events we wanted to directly test the capacity of sgRNAs 1, 2, 4 and 5 for their ability to induce DSB. T7 endonuclease cleaves double-stranded DNA at bases that are mismatched; mismatched bases are a result of indels produced from DSBs which are repaired via the non-homologous end joining pathway. Takayuki et al, developed a protocol to screen for the ability of sgRNAs to induce DSB using the T7 endonuclease on blastocysts derived from CRISPR/Cas9 micro-injections (Takayuki et al., 2014). As such we attempted this T7 endonuclease assay to determine which of our sgRNAs are capable of inducing indels, and thus are able to induce DSB. Microinjections performed at the CR-CHUM using a single sgRNA (sgRNA 2, 4 or 5 (used in rounds 1 thru 4) or sgRNA 3 or 6 (newly designed sgRNAs targeting intron 1 and 2 respective, see Fig 8 & Table 2)) and Cas9 endonuclease, embryos were then cultured *in vitro* to obtain blastocysts. The blastocysts were then provided to us for T7 endonuclease assay screening: 9 blastocysts from sgRNA 2-micro-injected, 1 from sgRNA 4, 13 from sgRNA 5, 4 from sgRNA 3 and 9 from sgRNA 6. These were screened using primer pairs F5R5 (wt = 228bp) and F6R6 (wt = 230bp) along with T7 endonuclease reaction followed by analysis on an agarose gel. Since we were only able to obtain a small volume of DNA from blastocysts, we were unable to optimize the assay and no clear endonuclease digestion products were observed. Albeit, we determined an estimate of the sgRNA cutting efficiency (number of 'blastocysts with indels' divided by 'total blastocyst screened') for each sgRNA analyzed based on the reduction in the wild-type amplicon intensity following T7 endonuclease treatment (which was not observed in the wild-type control) as an

indication of the presence of indels (Fig 9). The cutting efficiencies were 6/9 = 67% for sgRNA 2, 1/1 = 100% for sgRNA 4, 4/6 = 67% for sgRNA 5, 3/4 = 75% for sgRNA 3 and 4/5 for sgRNA 6. Based off of this, we chose to proceed with using sgRNA 2 and 3 to target intron 1 and sgRNA 5 and 6 to target intron 2 for subsequent micro-injections; despite the 100% cutting efficiency, we rejected sgRNA 4 since only one blastocyst was screened.

We also designed new repair templates 4 and 5 to complement the new panel of sgRNAs targeting *Tmed2* intron 1 and *Tmed2* intron 2 (Fig 8 & Table 3): the spacer sequence for the sgRNA which targets the region of the loxP insertion was deleted, while the PAM sequence of the other sgRNA binding site was mutated from 5' NGG 3' to 5' NTT 3' and two other bases within the spacer sequence proximal to the PAM sequence were also mutated in order to prevent Cas9:sgRNA-induced DSB after successful loxP integration.

3.4 A C3H:B6 genetic background mouse carries a *Tmed2* intron 1 loxP insertion

Microinjection rounds 5 and 6 used C3H:B6 mixed genetic background mice. A total of 48 mice were born and screened for indels in *Tmed2* intron 1 and 2; 31 mice from round 5 and 17 mice from round 6. 13 of 48 (27%) C3H:B6 mice screened positive for indel events in either intron 1 or intron 2 but never both introns; 5 of these mice were from microinjection round 5 and 8 mice were from round 6.

Microinjection round 5 used sgRNA 1, 2, 4 and 5 and repair template 1 and 2. Using primer set F2R2, 3 mice with events in *Tmed2* intron 1 were observed (Fig 11a): Mouse D carried an insertion slightly under 700bp, Mouse E carried an insertion event at slightly below 700bp and a small deletion below 600bp, and Mouse F also carried an insertion event at slightly below 700bp. Restriction digestion of the PCR products using EcoRI (based on repair template

1) did not reveal any digestion products (not shown). As such it was concluded that these mice do not carry a loxP site insertion in the targeted *Tmed2* intron 1 locus. Using primer set F4R4, the microinjection round 5 mice were screened for *Tmed2* intron 2 events, 2 mice carried intron 2 insertion events (which were not the same mice carrying intron 1 events): Mouse G and H both carried an insertion event at around 800bp (~170bp above the expected wild-type amplicon) which did not restriction digest using EcoRV (based on repair template 2) (not shown). To confirm the *Tmed2* intron 2 event, primer set F6R6 (wt = 230bp; loxP = 270bp), which amplifies a narrower region closer to the expected insertion site, was used to screen Mouse G and H. In addition to observing an insertion event at around 450bp, primer set F6R6 also revealed insertion events at around 270bp as expected for a loxP insertion event (Fig 11b). However, since the primer set F4R4 PCR product of Mouse G and H did not restriction digest, we speculated that either the insertion was not an intact loxP insertion or the designed EcoRV restriction site was mutated during homology-directed repair and the loxP may be intact.

To verify that the insertion events observed in microinjection round 5 does not correspond to an intact loxP insertion with a mutated restriction site. We Sanger sequenced the insertion resembling a loxP insertion (based on amplicon size) in intron 1 or intron 2 of Mouse E (Fig 11a) and Mouse H (Fig 11b), respectively. The bands on the agarose gel corresponding to the insertions were extracted and cloned into the pCR™II-TOPO vector and Sanger sequenced as previous described as in section 3.3. Surprisingly, sequencing of the Mouse E *Tmed2* intron 1 insertion revealed no insertion, rather, a small 12bp deletion was detected where the predicted insertion site is located (not shown). Sequencing of the Mouse H *Tmed2* intron 2 insertion revealed a 19bp partial loxP insertion corresponding to the 3'-end of the loxP sequence and a scrambled unrecognizable sequence upstream of the partial loxP insertion (not shown). This

confirms and explains that restriction digestion using EcoRV did not produce any restriction digestion products as a result of absence of an intact EcoRV restriction site. In summary, no complete loxP insertion was observed in *Tmed2* of mice from microinjection round 5.

Microinjection round 6 used sgRNA 2, 3, 5 and 6 and repair template 4 and 5 (Fig 8 & Table 2 and 3). 8 mice carried a variety of intron 1 indel events when screened using primer pair F2R2. Interestingly, one male mouse (Mouse I) carried a PCR amplification product which yielded the expected product sizes 298bp and 310bp when restriction digestion reaction was performed using EcoRI (Fig 10, left), strongly suggesting the proper insertion of the designed EcoRI and loxP sequence in *Tmed2* intron 1 (herein referred to as the *Tmed2*-loxP1 allele). As observed in the gel electrophoresis experiment, Mouse I had additional insertion and deletion events (Fig 9, left) reflecting a mosaic genotype at the *Tmed2* intron 1 locus. PCR screening with primer pair F4R4 revealed no products other than the wild-type allele of 634bp (not shown). Mouse I was chosen as a founder to start a colony in order to propagate the putative *Tmed2*-loxP1 allele to offsprings to generate *Tmed2*$^{loxP1/+}$ mice and confirm an intact loxP sequence by Sanger sequencing.

All in all, 13 of 48 (27%) C3H:Bl6 mice carried events in *Tmed2* (11 in intron 1 and 2 in intron 2). One of the *Tmed2* intron 1 event restriction digested according to designed repair template suggesting that the loxP site was properly inserted in intron 1.

3.5 Isolating and confirming the putative *Tmed2*-loxP1 allele

Mouse I (Fig 10, left), the *Tmed2*$^{loxP1/+}$ founder, was bred to wild-type C3H female mice and produced 21 G1 animals. These mice were similarly screened for *Tmed2*-loxP1 by PCR using primer set F2R2 and restriction digestion with EcoRI enzyme. We observed 7 mice (6

females and 1 male) carrying an insertion which produced a restriction digestion product at 300bp (comparable to the expected 298bp and 310bp, since the gel was not run long enough to segregate the two bands) (Fig 10, right). This confirms that the putative *Tmed2*-loxP1 allele is heritable. Additionally, *Tmed2* intron 2 was also screened in these mice using primer set F4R4 in order to test if any events occurring here could be inherited from Mouse I; all G1 mice carried only the wild-type amplicon size of 634bp (not shown). Thus, the putative *Tmed2*-loxP1 allele detected in Mouse I is germ-line transmittable and *Tmed2*$^{loxP1/+}$ were generated which does not carry any *Tmed2* intron 2 event detectable by PCR genotyping alone.

3 females (Mouse I1, I2, I3) and one male (Mouse I4) G1 mice were selected for sequencing to verify that the putative *Tmed2*-loxP1 insertion contains an intact loxP site. As the wild-type and *Tmed2*-loxP1 amplicon of primer set F2R2 are very close in size (591bp and 608bp, respectively) the PCR reaction (containing both amplicons) was sub-cloned into the pCR^{TM}II-TOPO vector in order to facilitate Sanger sequencing as in section 3.3. Aligning the nucleic acid sequence for Mouse I1 with repair template 4 revealed an intact EcoRI site and a T>C transition at the 6th nucleic acid position of the loxP site (Fig 12, top left). For Mouse I2 and I3, the alignment revealed an intact loxP sequence and EcoRI site (Fig 12, top right & bottom left). Mouse I4 aligned with repair template 4 revealed a G>A transition at the 9th nucleic acid position of the loxP sequence (Fig 12, bottom right). Overall, we generated two *Tmed2*$^{loxP1/+}$ female mice, but no male mice, with a confirmed intact *Tmed2*-loxP1. At the time of thesis preparation, these two *Tmed2*$^{loxP1/+}$ were used for breeding in order to generate *Tmed2*$^{loxP1/loxP1}$ male and female mice for future micro-injection experiments to target the insertion of a loxP site in *Tmed2* intron 2 and generate *Tmed2*$^{fl/fl}$ mice. We are also attempting to target the insertion of loxP site in *Tmed2* intron 3.

3.6 An intron 2-targeting sgRNA is capable of inducing Cas9-mediated DSB

In preparation for micro-injection experiments to insert a loxP site into *Tmed2* intron 2 of *Tmed2*$^{loxP1/loxP1}$ mice, the T7 endonuclease assay was performed on PCR products obtained using tail DNA of 9 of the C3H:Bl6 mice as DNA template originating from microinjection round 6 (microinjected with intron 2-targeting sgRNA 5 and 6; see Section 3.4)) and using primer set F4R4 (intron 2). This was to directly test whether sgRNA 5 and 6 could produce Cas9-mediated DSB in *Tmed2* intron 2 as no observable events were seen when screening this intron in micro-injection round 6 mice. Small indel events produced as a result of sgRNA 5-induced DSB is predicted to produce T7 endonuclease products of 239bp and 395bp and sgRNA 6, products at 281bp and 353bp. One of the nine screened mice had a F4R4 PCR amplicon which restriction digested into products at ~250bp and ~400bp (see 'Mouse J', Fig 13), suggestive of indel mutations located where sgRNA 5 is expected to cut. None of these mice carried T7 endonuclease products reflective of a sgRNA 6-induced indel mutation (see representative 'Mouse K', Fig 13). All T7 treated PCR products contained a digestion product ~50bp below the wild-type undigested amplicon (634bp) and at ~100bp which does not correspond to predicted sizes of indels occurring at the sgRNA 5 and 6 cut sites (see representative 'Mouse K', Fig 13); since all 9 samples carried this product, it was reasoned that this could be an off-target resulting from these mice being of mixed C3H:B6 genetic background. These results estimate that sgRNA 5 is capable of inducing DSB with an efficiency of 1/9 = 11% and sgRNA 6 does not induce DSB when both sgRNAs are simultaneously introduced by micro-injection into C3H:B6 embryos.

3.7 *Tmed2*$^{99J/+}$ present with deregulated proportion of hematopoietic cells in the liver at E17.5 liver but is abolished at P5

Murine liver development begins at around E9.5 with the appearance of a liver diverticulum which continues to grow until about 4 weeks postnatally to generate the mature adult organ (Crawford et al., 2010). *Tmed2* expression was detected at the onset of organogenesis in the mouse liver at E9.5 (Jerome-Majewska et al., 2010). In addition, western blot analysis of liver protein lysates revealed TMED2 expression at E17.5 and P5 in mice (unpublished data). These ages at which *Tmed2* expression was detected in the liver corresponds to ages at which liver development is occurring; thus, it is conceivable that *Tmed2* may participate in the formation of the organ. As such, we stained *Tmed2*$^{99J/+}$ liver sections using HE at E17.5 and P5, ages where we observed TMED2 expression, to test whether any morphological differences could be observed.

Four cell-types are distinguishable by morphology in the liver at E17.5 and P5 (Fig 14a): granulocytes, hepatocytes, red blood cells and megakaryocytes. For each sample, two slides (containing sections ~125um apart) were stained with HE and analyzed. The number of each cell type was counted from 3 representative images on each slide. The proportion of each cell type relative to total number of counted cells for any given sample was calculated from counts in all 6 images; the mean cell-type proportion among *Tmed2*$^{99J/+}$ and wild-type littermates grouped as males and females were compared using an ANOVA (sex as one source of variation and genotype as the other). At E17.5 no interaction between sex and genotype (*Tmed2*$^{99J/+}$ ♀ (n=6) and ♂ (n=4); *Tmed2* wild-type ♀ (n=8) and ♂ (n=9)) was observed for granulocytes (p=0.919), hepatocytes (p=0.851) and red blood cells (p=0.833). As such, the mean proportions of these cells-types were compared genotype-wise only (*Tmed2*$^{99J/+}$ (n=17); *Tmed2* wild-type (n=10)) within the ANOVA analysis (Fig 14b). *Tmed2*$^{99J/+}$ (57.7%) contained 3.1% more granulocytes

proportions compared to *Tmed2* wild-type (54.6%) livers (p=0.013). *Tmed2*$^{99J/+}$ (34.8%) contained hepatocyte proportions comparable to *Tmed2* wild-type (35.1%) livers (p=0.735). *Tmed2*$^{99J/+}$ (7.3%) contained 2.8% fewer red blood cell proportions compared to *Tmed2* wild-type (10.1%) livers (p=0.01). At E17.5, an interaction between sex and genotype was observed for megakaryocytes (p=0.025), as such differences between genotype were compared separately among sexes and a Sidak's multiple comparisons correction was applied. However, no difference was observed in megakaryocyte proportions between *Tmed2*$^{99J/+}$ (0.3%) and wild-type (0.2%) male livers (p=0.076) and *Tmed2*$^{99J/+}$ (0.2%) and wild-type (0.2%) female livers (p=0.455) (Fig 14b). Thus, *Tmed2*$^{99J/+}$ E17.5 livers have an increased proportion of granulocyte and reduced proportion of erythrocyte compared to age-matched wild-type livers.

The same analysis was performed for P5 livers (*Tmed2*$^{99J/+}$ ♀ (n=8) and ♂ (n=5); *Tmed2* wild-type ♀ (n=7) and ♂ (n=4)). No interaction between sex and genotype was observed for all cell-types using an ANOVA: granulocyte (p=0.131), hepatocyte (p=0.136), red blood cell (p=0.609), and megakaryocyte (p=0.404). No differences in any of the analyzed cell types were observed when comparing between *Tmed2*$^{99J/+}$ (n=13) and *Tmed2* wild-type (n=11) (Fig 14b): granulocytes (*Tmed2*$^{99J/+}$ (46.4%) and wild-type (44.3%), p=0.409), hepatocytes (*Tmed2*$^{99J/+}$ (50.1%) and wild-type (53.2%), p=0.238), red blood cells (*Tmed2*$^{99J/+}$ (3.4%) and wild-type (2.4%), p=0.135), and megakaryocytes (*Tmed2*$^{99J/+}$ (0.1%) and wild-type (0.1%), p=0.625). As such, the deregulated proportion of erythrocyte and granulocyte observed at E17.5 in *Tmed2*$^{99J/+}$ livers is no longer observed at P5 of age.

3.8 Peripheral blood of 3 month old male *Tmed2*$^{99J/+}$ and wild-type animals have comparable blood cell counts

Differences in granulocyte and red blood cell proportion was observed in *Tmed2*$^{99J/+}$ livers compared to wild-type control at E17.5 but not at P5. As such, we next tested whether circulating blood cell numbers differ between *Tmed2*$^{99J/+}$ and *Tmed2* wild-type adult mice (only male mice were analyzed). Complete blood count analysis revealed no statistically significant difference in white blood cell count (platelets, lymphocytes, monocytes and granulocytes (neutrophils and eosinophils)) and red blood cell counts *Tmed2*$^{99J/+}$ (n=5) compared to wild-type control (n=4) by Mann-Whitney U test (Fig 15). Thus, adult *Tmed2*$^{99J/+}$ mice do not have deregulated numbers of circulating blood cells.

3.9 mRNA expression of hematopoietic transcription factors do not differ between E14.5 livers of *Tmed2*$^{99J/+}$ and wild-type animals

We observed a change in representation of red blood cell and granulocyte proportions in the E17.5 of *Tmed2*$^{99J/+}$ livers (section 3.7) – these two cell types are derived from a common progenitor cell called the common myeloid progenitor (CMP) (Fig 1) (Friedman, 2002). It is thus possible that the cell proportion deregulation observed at E17.5 may be a result of deregulated development of the CMP. As such, we next tested the possibility of altered differentiation within the hematopoietic lineage by measuring the mRNA expression levels of hematopoietic transcription factors associated with the differentiation of hematopoietic progenitors (Fig 1) (Friedman, 2002) using RT-qPCR on liver mRNA of *Tmed2*$^{99J/+}$ compared to wild-type littermates: transcription factor PU.1 for granulocyte macrophage progenitor (GMP), Gata-1 for megakaryocyte erythrocyte progenitor and erythrocyte development (MEP), Jun for macrophage development, C/EBPε for granulocyte development, Gata-3 for T-lymphocyte development and Pax5 for B-lymphocyte development. We chose to perform the experiment on E14.5 livers as

this is the age in which hematopoiesis is at its peak within the liver and thus would be the optimal stage for observing potential differences (Crawford et al., 2010).

During dissection to obtain the E14.5 liver samples, no difference in embryo appearance was observed (not shown). No differences were observed in expression of tested transcription factors in E14.5 *Tmed2*$^{99J/+}$ compared to wild-type livers using a two-tailed unpaired t-test (Fig 16): Jun (p=0.489), Pax5 (p=0.951), Gata-3 (p=0.298), C/EBPε (p=0.211), Gata-1 (p=0.935) and PU.1 (p=0.203). All in all, no difference in expression of transcription factors associated with the development of hematopoietic cell was observed within the liver during the peak of hepatic hematopoiesis.

Additionally, we measured the expression level of *Tmed2* in these E14.5 liver mRNA. No differences in *Tmed2* mRNA expression (Fig 16) was observed (two-tailed unpaired t-test, p=0.860) which reflects what was previously observed for the *Tmed2* 99J line (Hou et al., 2017; Jerome-Majewska et al., 2010).

3.5 Bleeding defects were not detected in adult *Tmed2*$^{99J/+}$ males

TMED2 was previously shown to be involved in the trafficking of thrombin receptors PAR-1 and PAR-2 in HEK293 and rat astrocyte cells (Luo et al., 2007, 2011). PAR-1 and PAR-2 are involved in the activation and maintenance of the platelet coagulation response. Thus, defects leading to greater activation of PAR-1 or PAR-2 trafficking could lead to altered platelet coagulation which may lead to thrombosis. Thrombosis has been associated with NAFLD – a study reported that 47.5% of a cohort of NAFLD patients also presented with portal vein thrombosis (Basaranoglu et al., 2016). *Tmed2*$^{99J/+}$ adult mice 6 months of age and older were

observed to develop NAFLD at a greater frequency compared to littermates (Hou et al., 2017). As such a possible phenotype that may be present in *Tmed2*$^{99J/+}$ mice is defective coagulation.

In order to test if *Tmed2*$^{99J/+}$ animals may have a defect in coagulation, we chose to perform a tail bleeding assay to assess whether *Tmed2*$^{99J/+}$ adults bleed differently compared to wild-type controls. The bleeding assay was performed on young animals (*Tmed2*$^{+/+}$ (n=7) and *Tmed2*$^{99J/+}$ (n=12); 3-4 weeks old) and older animals (*Tmed2*$^{+/+}$ (n=4) and *Tmed2*$^{99J/+}$ (n=5); 10-13 weeks old male mice only). No correlation was observed between weight of animals and initial bleeding duration (r=0.303) (Fig 17a). No differences in initial bleeding duration were observed (two-tailed unpaired t-test) in young (p=0.858) and in older (p=0.552) *Tmed2*$^{99J/+}$ compared to wild-type animals (Fig 17b). Since TMED2 has been associated with the trafficking of thrombin receptor PAR-2, we also compared the mRNA expression of Par-2 in using RT-qPCR. No difference in expression was observed between E14.5 *Tmed2*$^{99J/+}$ (n=8) and *Tmed2*$^{+/+}$ (n=5) livers using a two-tailed unpaired t-test (p=0.707) (Fig 18). All in all, no evidence suggesting that *Tmed2*$^{99J/+}$ animals present with bleeding defects prior to 10 weeks of age was found.

CHAPTER 4

Discussion

TMED2 is a cargo receptor protein involved in vesicular transport. Our lab previously demonstrated, in the murine *Tmed2* null 99J model, that a complete knock-out results in embryonic lethality as a result of malformation of the placenta before E11.5 and that prior to death these embryos exhibit developmental delay as early as E8.5 (Jerome-Majewska et al., 2010). Thus, TMED2 plays a crucial role in development separate from its role in the formation of the placenta and it is possible that this role may extend into organogenesis (post-E11.5). Western blot using anti-TMED2 antibody on E17.5 liver protein lysates reveals expression within the liver (unpublished data), which suggests that TMED2 can have a function during this age. Since embryonic lethality precludes the analysis of $Tmed2^{99J/99J}$ mutants beyond E11.5, in order to study the role of TMED2 during organogenesis, an alternative to complete KO must be developed. The *Cre*/loxP system was demonstrated to be an effective method for deleting a gene locus (Gu et al., 1993). My project aimed to develop a *Tmed2* cKO allele by flanking *Tmed2* exon 2 with loxP sites using CRISPR/Cas9 to promote loxP insertion. I was able to accomplish a single loxP insertion in *Tmed2* Intron 1(Fig 10 and Fig 12b, c). However, in order for the conditional gene-targeting to function, a second loxP site will be required in *cis* with the currently inserted *Tmed2* intron 1 loxP site. We are currently attempting to insert this second loxP site in either *Tmed2* intron 2 or intron 3.

In this study, we targeted loxP insertion in *Tmed2* intron 1 and intron 2 using the same CRISPR/Cas9-mediated HDR strategy. Out of a total of 93 mice originating from micro-injections, 15/93=16% of mice carried intron 1 events whereas only 2/93=2% carried intron 2 events. This could be a result of the intron 2-targeting guides not producing DSB effectively, repair templates not being used during repair of the DSB and/or that *Tmed2* intron 2 is protective against genetic edits – since my project was not to characterize and optimize CRISPR/Cas9

based editing, the proper experiments were not performed to enable the differentiation between these possibilities. However, this raises the concern of variability in success rate of knock-in experiments within a single gene and its impact in targeting insertions using CRISPR/Cas9. Unravelling and optimizing a protocol for identifying such parameters could improve the use of CRISPR/Cas9 as a genome-editing tool for gene manipulation.

The successful insertion of a single loxP into *Tmed2* intron 1 complements what other groups were able to accomplish (Ma et al., 2017). This further validates the use of CRISPR/Cas9 in generating gene edits for the study of gene functions. However, as observed in the current study, the frequency of successful loxP insertion was very low (1/93=1.1%), leaving room for improvement in this CRISPR/Cas9 strategy. One method that would be interesting to investigate is to test different genetic mouse strains to observe which strain may be more permissive to genomic edits induced by CRISPR/Cas9. In the current study, 1/7=14.3% CD1 mice, 4/38=10.5% CD1:FvB and 11/48=22.9% C3H:B6 would suggest that C3H:B6 genetic background is more favourable. In addition, the C3H:B6 genetic background mice were the ones where we successfully inserted a loxP site in intron 1 (Fig 10 & 12). Albeit, since the current study was not designed to investigate this hypothesis, it is difficult to arrive to a definitive conclusion since some of the sgRNA and repair templates were changed between the genetic strains used.

While genotyping for insertions in G1 population mice generated from crosses with CRISPR/Cas9 microinjected founders, we had observed some samples with a third PCR product above the expected bands (Fig 5b) or, in the *Tmed2*-loxP1 mice, a top band that is undigested along with the expected wild-type product (Fig 10, right) despite these mice being heterozygous (wild-type allele and *Tmed2*-insertion allele). In the same experiment, the wild-type control

showed only the expected amplicon, suggesting that the PCR reaction was optimized for the wild-type allele. A possible explanation for this phenomenon is that the third amplicon is an off-target generated as a result of the PCR conditions being suboptimal for the *Tmed2* allele carrying an insertion. However, an alternative explanation could be that the third amplicon corresponds to a complex between the wild-type allele with the *Tmed2*-insertion allele; most of the sequence would be homologous save for the stretch of inserted sequence which would have no complementary DNA sequence to base pair with. The reason for this amplicon appearing larger in size compared to the other alleles is that this complex would form a secondary DNA structure which travels through agarose gel pores less efficiently. Additionally, this would explain why this structure was not digested with EcoRI (Fig 10, right). This hypothesis could be verified by running an alkaline agarose gel electrophoresis (Sambrook and Russell, 2006) which will show only two bands if the third amplicon corresponds to a complex of wild-type and *Tmed2*-insertion alleles and three bands if the third band corresponds to a non-specific or off-target amplification.

In the CRISPR/Cas9 microinjection experiments, we also attempted to use a larger double-stranded repair template (repair template 3; Fig 3b & Table 3) with the prediction that it could lead to the insertion of both loxP sites in a single step (since it contains additional homologous sequences and carries both loxP sites). However we did not observe a greater frequency of successful edits. This result is in accordance with a group which demonstrated that a double stranded DNA repair donor was not as effective as single stranded DNA repair donors in knock-in experiments (Richardson et al., 2016). Richardson et al. also demonstrated that the stranded-ness (whether the single-stranded DNA donor was complementary or identical to the sgRNA spacer sequence) is also an important consideration.

Once *Tmed2*$^{fl/fl}$ mice have been generated, it would allow us to knock out TMED2 in a temporally and spatially-specific manner depending on where *Cre*-recombinase is expressed – this is often achieved by the expression of *Cre* under tissue-specific gene promoters. For the purposes of studying the involvement of TMED2 within the developing liver, alb*Cre* transgenic mice will be used to generate *Tmed2*$^{alb/alb}$ mice. Alb*Cre* transgenic mice express *Cre* in hepatocytes (Weisend et al., 2009) as early as E10.5-11.5 (Crawford et al., 2010; Serls et al., 2005). The role of the liver between E11.5 and birth is mainly to expand and differentiate the pool of hematopoietic progenitor cells from the yolk sac (Crawford et al., 2010). Thus, a potential phenotype that may be observed is a perturbed hematopoietic lineage differentiation if hepatocytes do not develop properly as a result of liver-specific removal of TMED2. The cell proportion analysis in this study revealed the presence of deregulated red blood cell and granulocyte proportions in *Tmed2*$^{99J/+}$ livers which supports that TMED2 may play a role in hematopoietic lineage development (Fig 14). However, no differences were observed in the expression of transcription factors GATA-1, GATA-3, PU.1, PAX5, C/EBPε and Jun important for hematopoietic progenitor cell differentiation (Fig 16). The reason for the defect in cell proportion may be a result of differences further downstream along the differentiation pathway or, alternatively, it may be a result of delayed exit of granulocytes from the liver parenchyma. A potential candidate for defects in granulocyte exit from the liver parenchyma is insulin-like growth factor 1 (IGF1). It was observed that hepatocyte-specific KO of IGF-1 leads to a decrease in the myelopoietic compartment of the spleen of 4 week old mice which was associated with an increase in the myelopoeitic compartment in the bone marrow and decreased circulating IGF-1 levels (Welniak et al., 2004). Following expansion in the fetal liver, hematopoietic progenitors exit the liver to populate the bone marrow and the spleen. The first follow-up experiment to

perform would be to test if *Tmed2*$^{99J/+}$ have altered circulating IGF-1 levels as outlined by Yakar et al. (Yakar et al., 1999). If TMED2 is involved in the secretion of IGF-1, defects observed in TMED2 mutant mice granulocyte proportions at E17.5 (Fig 14) could be associated with a decrease in spleenic myeloipoiesis. An interesting experiment to perform would be to analyze the spleen of *Tmed2*$^{alb/alb}$ and *Tmed2*$^{99J/+}$ embryos at E17.5 using colony forming assays to test whether myelopoiesis (CFU-GM) is altered as outlined by Welniak et al. (Welniak et al., 2004).

It is uncertain what the ramifications of the perturbed cell proportions at E17.5 may be. The difference was no longer present at P5 of age and circulating adult blood cell numbers do not seem to differ (Fig 14 and 15). Additionally, a caveat to analyzing cell types present within the liver using HE stained sections is that the cells may only be distinguished based on morphology. For cells with distinct morphology and staining (ex. Red blood cells, megakaryocytes and hepatocytes) HE stain provides a relatively decent method for assessing cell numbers, however for granulocytes, we are unable to differentiate between the specific sub-type of granulocytes (i.e. neutrophils, basophils and eosinophils) as well as from different hematopoietic progenitor cells. Thus the proportion analysis performed at E17.5 would benefit from confirmation from experiments such as flow cytometry to specifically measure the abundance of these cells based on cell surface markers. Alternatively, colony forming assay could be performed by plating cells from the liver on a petri-dish and culturing with growth factors (previously established by Welniak et al., 2004) and counting the number of colony forming unit granulocyte macrophage (CFU-GM) as well as burst forming unit erythroid (BFU-E) (Welniak et al., 2004) in order to assess myelopoietic and erythropoietic potential.

It was previously discovered that Emp24, the TMED2 *Drosophila* homologue, interacts with and traffics Wg in the early secretory pathway (Buechling et al., 2011; Li et al., 2015; Port

et al., 2011). Since Wg mutation leads to defects in *Drosophila* wing disc development when Emp24 is knocked-down (Buechling et al., 2011; Port et al., 2011), it is conceivable that a similar interaction may occur in vertebrates between TMED2 and Wnt-1 (the vertebrate Wg orthologue (Swarup and Verheyen, 2012)). Thus, it would be of interest to study whether or not TMED2 interacts with Wnt-1 protein and whether or not this interaction is important during embryonic development. *Wnt-1* mutation in mice leads to defects in the development of the midbrain and cerebellum (McMahon and Bradley, 1990). Notably, the rostral portion of TMED2 E9.5 99J homozygous mutant embryos (Jerome-Majewska et al., 2010) resembles E9.5 *Wnt-1* homozygous mutants (McMahon and Bradley, 1990). The rostral defects (cerebellar and midbrain) observed in the *Tmed2*$^{99J/99J}$ mutants could be explained by the deregulation of Wnt-1 trafficking; in this model, other defects in the 99J homozygous mutant would be a result of TMED2 trafficking of non-Wnt-1 cargo proteins. If protein-protein interaction between TMED2 and Wnt-1 is confirmed, it would additionally be interesting to use the *Tmed2*$^{fl/fl}$ to remove TMED2 in *Wnt-1*-expressing cells by crossing *Tmed2*$^{fl/fl}$ mice with *Wnt-1*-Cre transgenic mice. The predicted outcome of this is a phenotype resembling the midbrain and cerebellar defects observed in *Wnt-1* null mice (McMahon and Bradley, 1990).

CHAPTER 5

Tables and Figures

Gene	Forward Primer (5' -> 3')	Reverse Primer (5' -> 3')
Actb	CTCTGGCTCCTAGCACCATGAAGA	GTAAAACGCAGCTCAGTAACAGTCCG
Sdha	GCTGTGGCCCTGAGAAAGATC	ATCATGGCCGTCTCTGAAATTC
B2m	ATGCTATCCAGAAAACCCCTCAA	GCGGGTGGAACTGTGTTACG
Par-2	CTCAGAGTAGGGCTCCGAGT	TGTTGTTGCGTCCCGGTG
Gata-1	TGGCTGAATCCTCTGCATCA	CACCTGAAAGACTGGGGAGTG
PU.1	TGTCACCCCAAGGGGACTAT	CCAAGTCATCCGATGGAGGG
Pax5	GGACCATCAGGACAGGACAT	TGGCGTTTGTACTCAGCGAT
Gata-3	CCATTACCACCTATCCGCCC	CACACTCCCTGCCTTCTGTG
C/EBP ε	TGGCATCTACAGCAACCCAG	ACAGGGGCCTTGAGGACA
Jun	CAAGTGCCGGAAAAGGAAGC	GCTGCGTTAGCATGAGTTGG
Tmed2	CGGACAACAGGAGTACATGGAAGTCCG	GACCAAAGGACCACTCTGCTGT

Table 1 Primers used in RT-qPCR experiments.

Primers for the bolded genes were designed in a previous study (Wenyang et al., 2017).

Target *Tmed2* Intron	sgRNA	Sequence (5' -> 3')	Repair Template	Used in Micro-Injection Round…
Intron 1	sgRNA 1	AGGGAGCCAGTGTACA CTTT**GGG**	1 and 3	1, 2, 3, and 4
	sgRNA 2	CAGGGAGCCAGTGTAC ACTT**TGG**	1, 3 and 4	1, 2, 3, 4, 5 and 6
	sgRNA 3	TCACAGGAAAAATATCC AAT**AGG**	4	5 and 6
Intron 2	sgRNA 4	CTGTTACCTGGCTGATC CTG**GGG**	2 and 3	1, 2, 3, and 4
	sgRNA 5	CGTGGACCCCAGGATCA GCC**AGG**	2, 3 and 5	1, 2, 3, 4, 5 and 6
	sgRNA 6	ACAGTAACATCCACTTC AAC**AGG**	5	5 and 6

Table 2 List of sgRNA used for the generation of *Tmed2*$^{fl/fl}$ cKO mice.

Bold and underlined sgRNA sequences indicate the 3-nucleotide PAM sequence, the remaining sequence is the spacer sequence of the sgRNA.

Repair Template	Target *Tmed2* Intron	Sequence (5' -> 3')
1	Intron 1	ACTGTTGACTCTGTGCTAGTTTGATTTAAGTGGG AGAGTTAGTG**CCCA**AAGTGTA*gaattc*ataacttcgtatagc atacattatacgaagttatCACTGGCTCCCTGTAGGGGGACC TACTCAAGTTCCAGCCTATTGGATATT
2	Intron 2	CTGCTCATGTAAATCCCCAGACTCCATGGCCCTG GGTTCTGTTA**CCT**GGCTGATC*gatatc*ataacttcgtatagcat acattatacgaagttatCTG**GGG**TCCACGTGTACCTCTGTT TCTGTTTGCAGACATGCTAGCTTAGC
3	Intron 1 and 2	TGACTCTGTGCTAGTTTGATTTAAGTGGGAGAGT TAGTG**CCCA**AAGTGTA*gaattc*ataacttcgtatagcatacattata cgaagttatCACTGGCTCCCTGTAGGGGGACCTACTC AAGTTCCAGCCTATTGGATATTTTTCCTGTGAGG ATGCTGCTAAAGATCCTAAATGTTTAGTGAGTTT TCTGTTTCTCTCCTGCCTCCAGATCACAGGACCA GATAATAAAGGAATCTATAAAGGAGACCGGGAG TCCAGCGGGAAGTACACATTTGCAGCCCACATG GATGGGACATACAAGTTCTGCTTTAGCAATAGGA TGTCCACTATGACTCCAAAGATAGTAATGTTCAC CATTGACATTGGGGAGGCTCCCAAAGGACAAGA CATGGAGACAGAAGGTGAGGTGTCTCTTTGGACT CAGAGCTCATCTCAGTTCAGTTCACTCATCCATC TTAGTACTGTGTGTGTGACTTTCTCTCCAGATTCA TGTCTTAAAAACAAAATTCCTGTTGAAGTGGATG TTACTGTCTATTGTCAGTGATTTTGGTTGTGCCTT CTGGCAGCCATGAGTCACTCTGCTCATGTAAATC CCCAGACTCCATGGCCCTGGGTTCTGTTA**CCT**GG CTGATC*gatatc*ataacttcgtatagcatacattatacgaagttatCTG**G GG**TCCACGTGTACCTCTGTTTCTGTTTGCAGACA TGCTAGCTTAGC
4	Intron 1	TGAAGAGGTGTTTTAGGGAACTGTTGACTCTGTG CTAGTTTGATTTAAGTGGGAGAGTTAGTGC*gaattc*a taacttcgtatagcatacattatacgaagttatTAGGGGGACCTACTC AAGTTCCAG**AA**T**T**ATTAGACATTTTTCCTGTGAGG ATGCTGCTAAAGATCCTAAATGTTTAGTGAGTTT TCTGTTTCTCT
5	Intron 2	CATGTCTTAAAAACAAAATT**AA**T**T**GTTAAACTGGA TGTTACTGTCTATTGTCAGTGATTTTGGTTGTGCC TTCTGGCAGCCATGAGTCACTCTGCTCATGTAAA TCCCCAGACTCCATGGCCCTGGGTTCTGTTAataact tcgtatagcatacattatacgaagttat*tctaga*TGTACCTCTGTTTCT GTTTGCAGACA

Table 3 List of repair templates used for the generation of *Tmed2*$^{fl/fl}$ cKO mice.

Lowercase letters and yellow highlight indicate restriction site and loxP sequence (italicized sequence represent restriction sites). Underlined sequence represent sgRNA sequences, bold sequences represent sgRNA PAM sequence. Red sequence represents designed mutations in

sgRNA sequence to prevent sgRNA recognition after repair. For repair template 4 and 5, the sgRNA binding site located at location of the restriction site-loxP sequence was completely deleted.

Gene	KO Phenotype	Expressed in the E14.5 Liver
C/EBPε	(-/-) Impaired neutrophil and eosinophil development and myelodysplasia. Animals are susceptible to secondary bacterial infections	Weak expression in the liver at E14.0 (cell type not specified) observed by Northern and RT-PCR (Williams et al., 1998)
Gata-1	(+/-) most males die mid-gestation with blocked erythroid development; females survive birth, exhibit varying degrees of anemia and impaired hematopoiesis (-/-) female nulls exhibit varying degrees of anemia and impaired hematopoiesis	Moderate-Strong regionalized expression at E14.5 (more on periphery of liver) (cell type not specified) by RNA in situ. (Diez-Roux et al., 2011; Visel et al., 2004)
Jun	(-/-) death by midgestation with impaired hepatogenesis, altered fetal liver erythropoiesis and edema. (mutant) two serines to alanines; viable, fertile but small size	Moderate expression at E14.5, regionalized (boarder of liver, speckles throughout liver) (cell type not specified) by RNA in site (Visel et al., 2004)
PU.1	(-/-) may be fetal/perinatal lethal. Absence of myeloid and B cells and altered T and NK cell development. (hypomorphic allele) impaired B and myeloid development. T cell lymphomas and acute myeloid leukemia and die prematurely	Moderate expression at E14.5 regionalized (speckles throughout liver) (cell type not specified) by RNA in situ (Visel et al., 2004)
Gata-3	(-/-) Embryonic lethal with a variety of defects. T-cell development is impaired when the locus is conditionally KOed. Hair loss in spontaneous mutation	Weak expression at E14.5 regionalized. Cell type not specified by RNA in situ (Visel et al., 2004)

Table 4 KO phenotype and E14.5 liver expression of analyzed hematopoietic transcription factors.

All information was found via MGI.

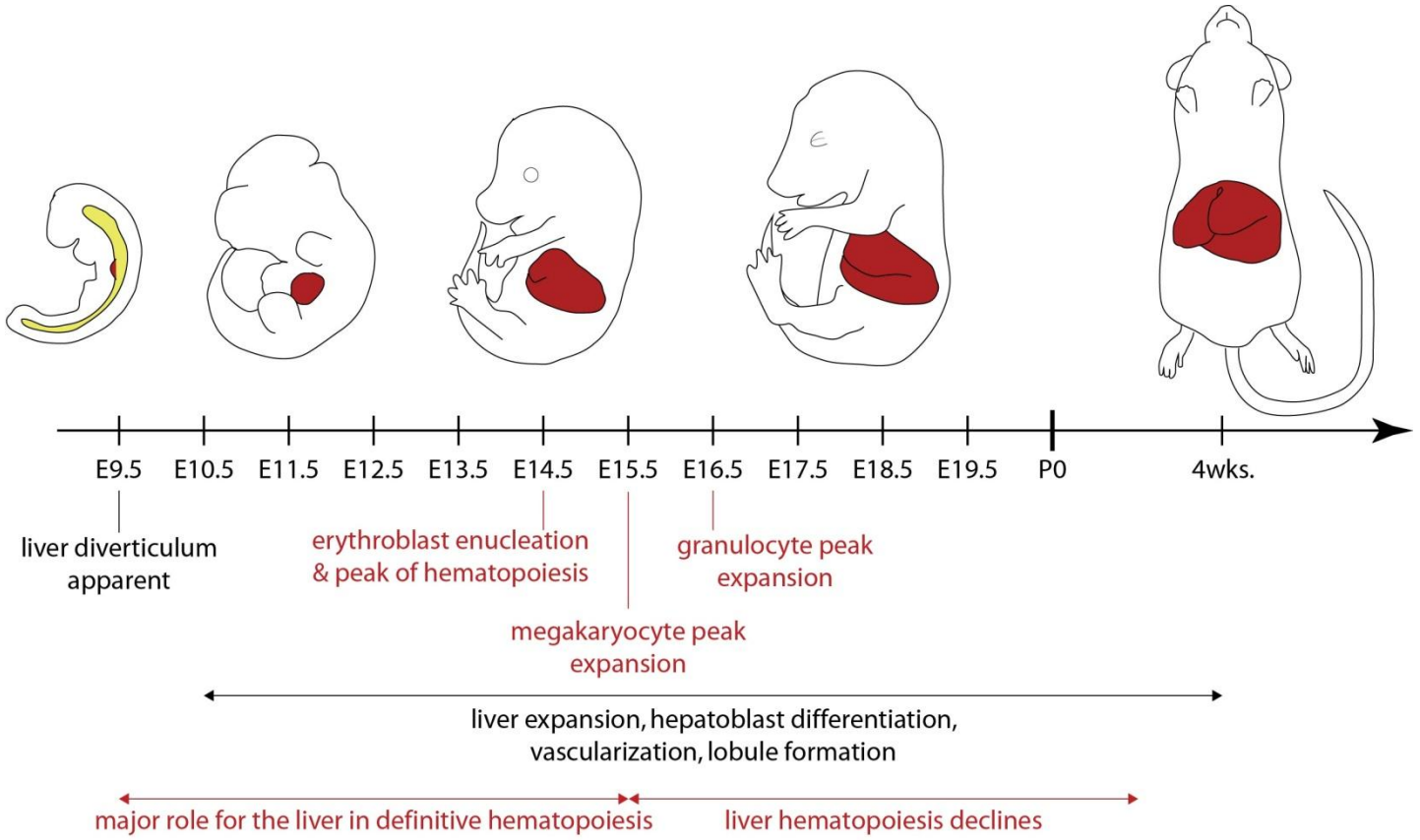

Figure 1 Murine liver development and embryonic liver hematopoiesis

Diagram demonstrating the timeline of murine embryonic liver development and major hematopoietic events. The endoderm is color-coded yellow at E9.5 and the liver is color-coded red throughout the diagram. Illustrations depict murine embryos from a lateral perspective (E9.5-E18.5) and the mature mouse at 4 weeks (4wks) of age post-natally from a ventral perspective. The liver diverticulum buds from the ventral part of the caudal foregut endoderm at E9.5 and expands in size until 4wks of age post-natally while hepatoblasts are differentiating, the liver is vascularizing and hepatic lobules are forming. The liver partakes in definitive hematopoiesis starting as early as E9.5 reaching a peak at E14.5 and declining after E15.5: enucleation of erythroblasts can be observed at E14.5, megakaryocyte precursor expansion peaks at E15.5 and granulocyte precursor expansion peaks at E16.5.

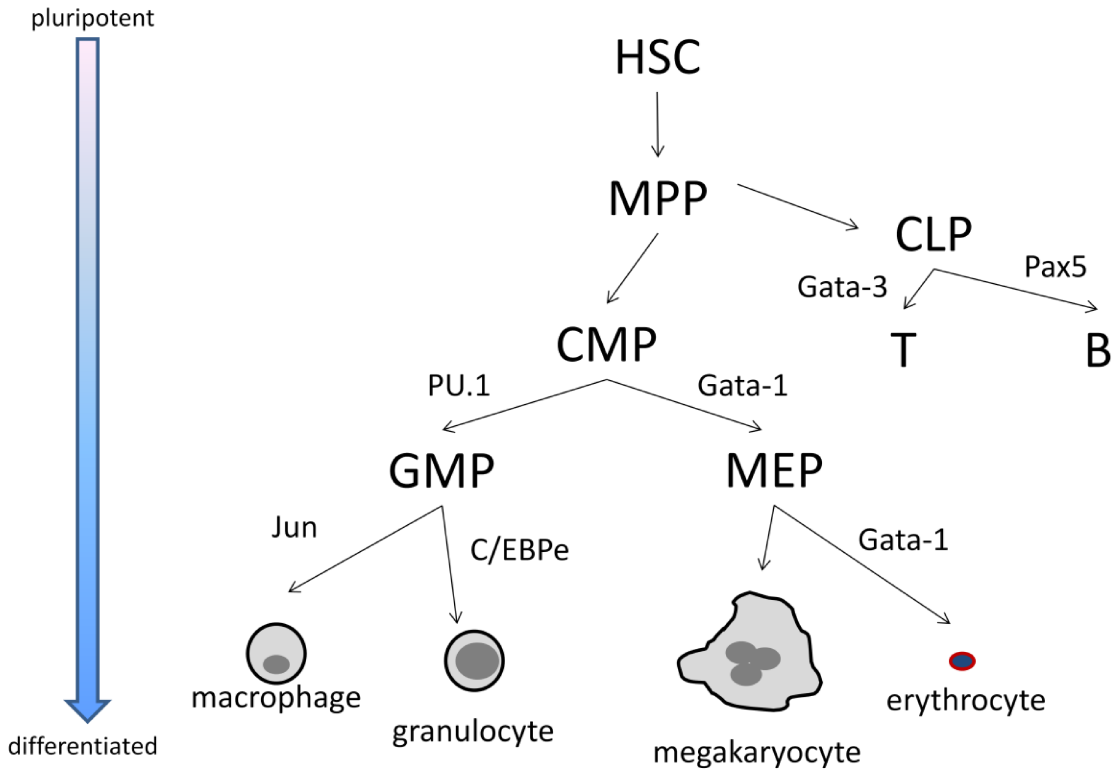

Figure 2 Hematopoietic lineage progenitor differentiation.

Small solid arrows, indicate cellular differentiation. Placed next to the small solid arrows are transcription factors involved in the development and differentiation step indicated by the arrow. HSC; hematopoietic stem cell, MPP; multipotent progenitor, CLP; common lymphoid progenitor, CMP; common myeloid progenitor, GMP; granulocyte-macrophage progenitor, MEP; megakaryocyte-erythrocyte progenitor, T; T-cell progenitor, B; B-cell progenitor.

(a)

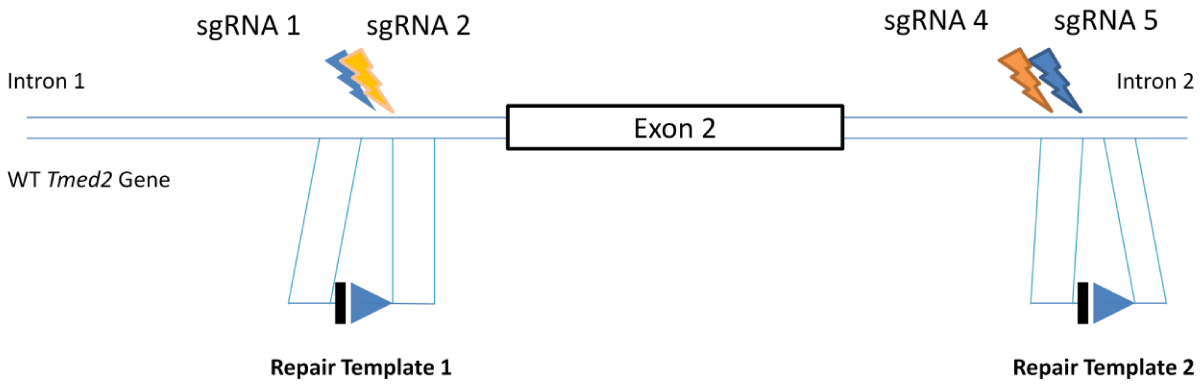

(b)

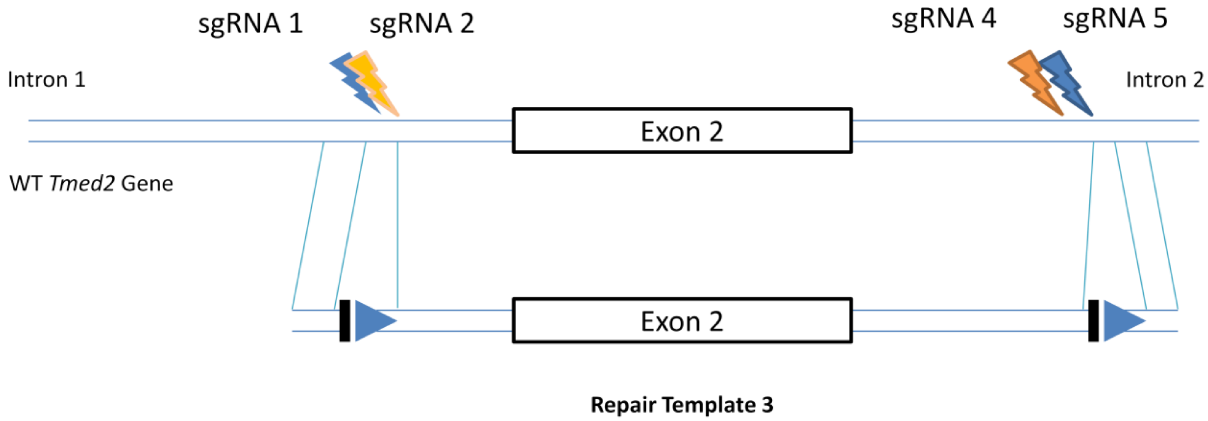

Figure 3 Diagram representing repair templates and sgRNAs used for CRISPR/Cas9 microinjection round 1 thru 5.

(a) Repair template 1 and 2 and (b) repair template 3 are juxtaposed with *Tmed2* exon 2 and surrounding intron 1 and 2 regions to show homologous regions. Lightning bolts indicate the *Tmed2* region where the indicated sgRNA is predicted to cut. The black rectangle in the repair templates indicate a restriction site (Repair template (RT) 1= EcoRI; RT 2 = EcoRV; RT3 = EcoRI (left) and EcoRV (right)). The blue triangle in the repair template indicate a loxP site. All other features in the repair templates indicate homologous regions to the wt *Tmed2* gene. For the sequence of each repair template see Table 3.

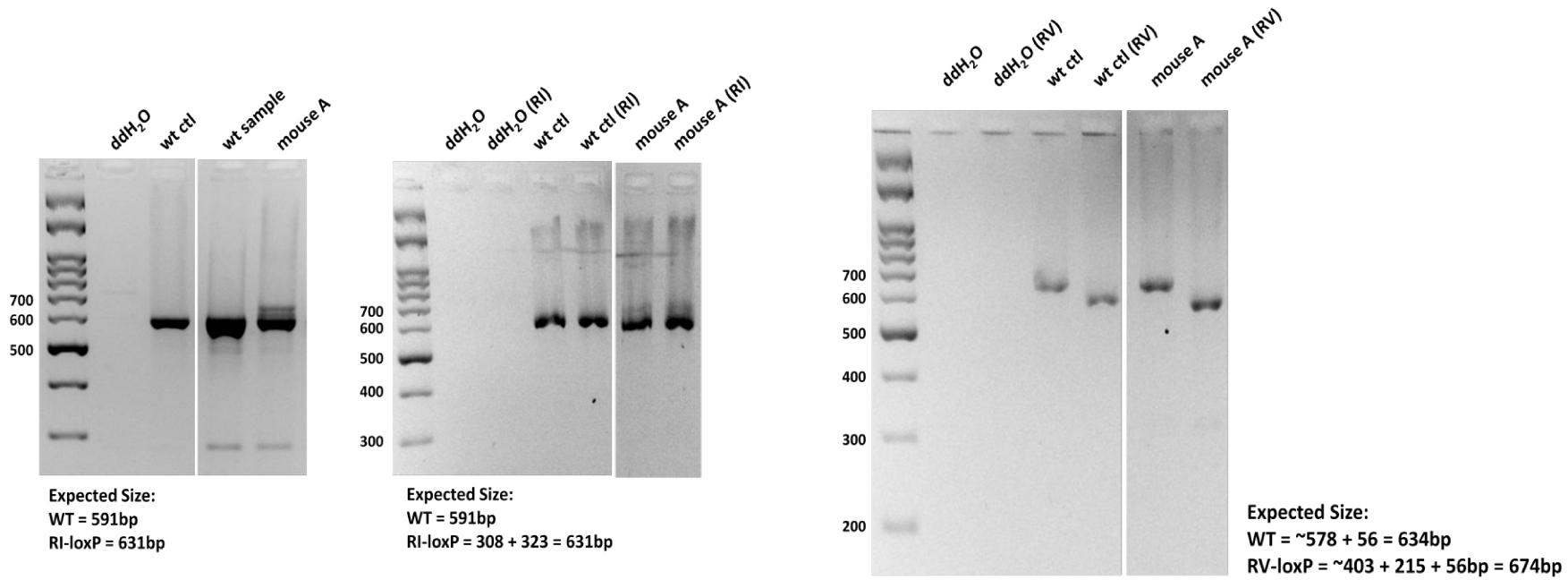

Figure 4 Representative gel electrophoresis for genotyping CD1 CRISPR/Cas9 microinjected mice demonstrates events in *Tmed2* intron 1 which was not a loxP insertion.

Left; representation of PCR screening for *Tmed2* intron 1 loxP insertion using primer pair F2R2 of microinjected CD1 mice. Middle; representation of *Tmed2* intron 1 PCR screening using F2R2 with EcoRI restriction enzyme digestion. Right; representation of PCR screening for *Tmed2* intron 2 loxP insertion using primer pair F4R4 with EcoRV restriction enzyme digestion of microinjected CD1 mice.

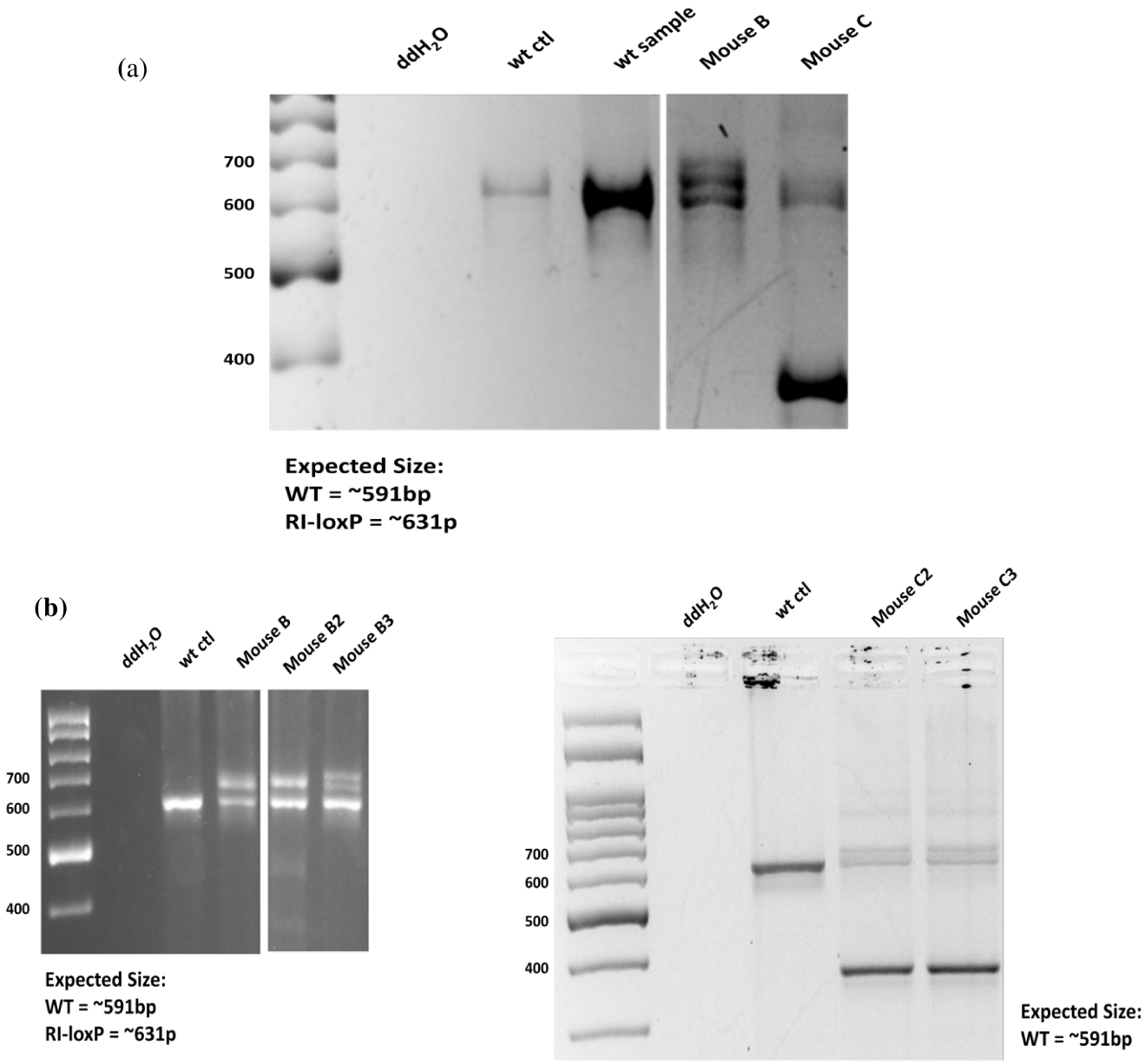

Figure 5 Representative gel electrophoresis for genotyping of CD1:FvB CRISPR/Cas9 microinjected mice demonstrates non-loxP insertion events in *Tmed2* intron 1

(a) Representative of PCR screening for a *Tmed2* intron 1 loxP insertion using primer pair F2R2 CD1:FvB mice from microinjections. Mouse B carries an insertion event above the expected 591bp wt *Tmed2* amplicon and Mouse C carries a deletion event below 400bp. (b) Representative PCR screening using primer set F2R2 for mice generated from mating Mouse B (left) or Mouse C (right) with wt C3H mice.

(a)

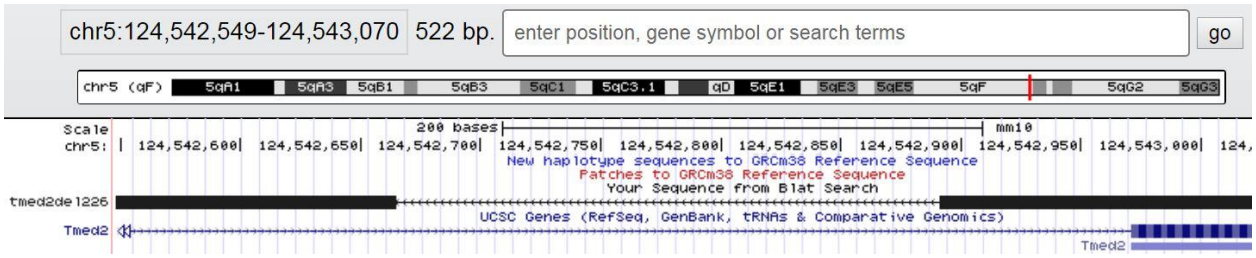

(b)

Genomic chr5 (reverse strand):

```
cctcaccttc tgtctccatg tcttgtcctt tgggagcctc cccaatgtca  124543121
atggtgaaca ttactatctt tggagtcata gtggacatcc tattgctaaa  124543071
GCAGAACTTG TATGTCCCAT CCATGTGGGC TGCAAATGTG TACTTCCCGC  124543021
TGGACTCCCG GTCTCCTTTA TAGATTCCTT TATTATCTGG TCCTGTGATC  124542971
TGGAGGCAGG AGAGAAACAG AAAACTCACT AAACATTTAG GATCTTTAGC  124542921
AGCATCCTCA CAGGAAAAAT ATCCAATAGg ctggaacttg agtaggtccc  124542871
cctacaggga gccagtgtac actttgggca ctaactctcc cacttaaatc  124542821
aaactagcac agagtcaaca gttccctaaa acacctcttc actctttatc  124542771
ctttaggtat tacctgtcca agcgaaatgt aaacctctca gaaagagaag  124542721
caggacaact ctccacatgg cctccaactg tctaacttca acaaaaactg  124542671
gcaagGCTGA AATCACAACC TAGGAACAAA GTTTTCCTAA ATGAGTAATT  124542621
TTATTTATTT TTGATTTGAG ATAGGGTCTC ATTACTGGTC CAAACTGGGT  124542571
TCAGATTCAG AGATCCAGCG ACctgtcttg aatgcgggat taaaagtgtg  124542521
cccaaggcca ttgattctcc tgcaggagac caaagccctt ctcaggcccc  124542471
atcccagtag ccactcgcca ct
```

Figure 6 Sanger sequencing reveals a 226bp deletion in *Tmed2* intron 1 of Mouse C2.

(a) Snapshot of the results from an alignment of the sequenced deletion event (see Fig. 4b, right) to the *Tmed2* gene (RefSeq Accession: NM_019770) using the UCSC Genome alignment tool. (b) Segment of sequence of *Tmed2* intron 1 alignment in (a) from UCSC Genome alignment results. Capitalized blue nucleic acids: matched bases; Lower case black nucleic acids: unmatched bases; Light blue nucleic acids: boundaries of gaps in either query or subject sequence.

(a)

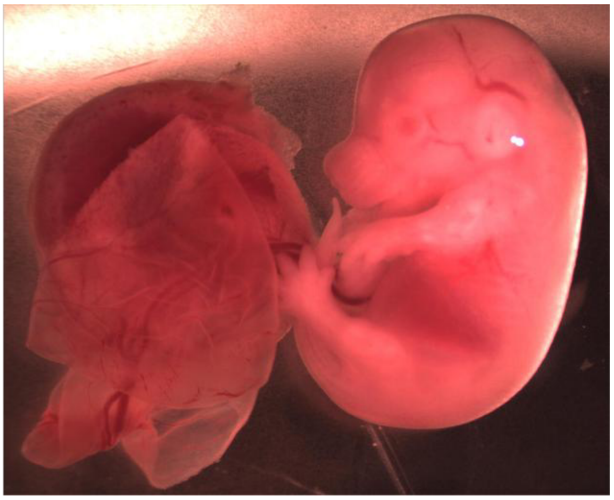

*This embryo was genotyped to be *Tmed2*$^{99J/\Delta226}$

(b)

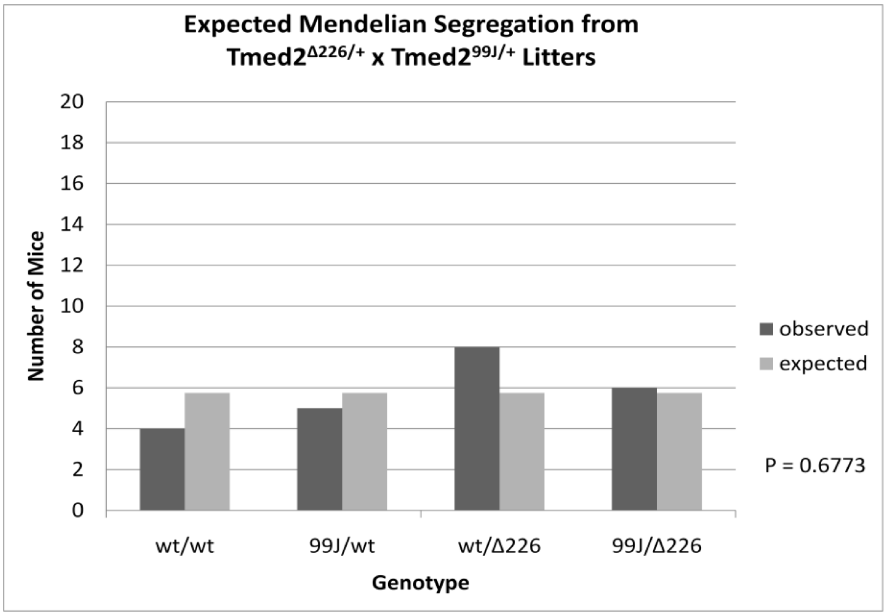

Figure 7 *Tmed2*$^{99J/\Delta226}$ E14.5 embryos appear normal and embryos and mice are present in expected Mendelian ratio.

(a) Image of an embryo dissected at E14.5, representative of all mice from the entire litter. This embryo was genotyped to be *Tmed2*$^{99J/\Delta226}$. Structure on the left is the placenta underneath the yolk sac. (b) Bar graph showing the observed numbers of each genotype from two *Tmed2*$^{99J/+}$ x *Tmed2*$^{+/\Delta226}$ crosses compared to predicted numbers of each genotype based on Mendelian segregation. Chi-Squared goodness of fit test was performed (p=0.6773).

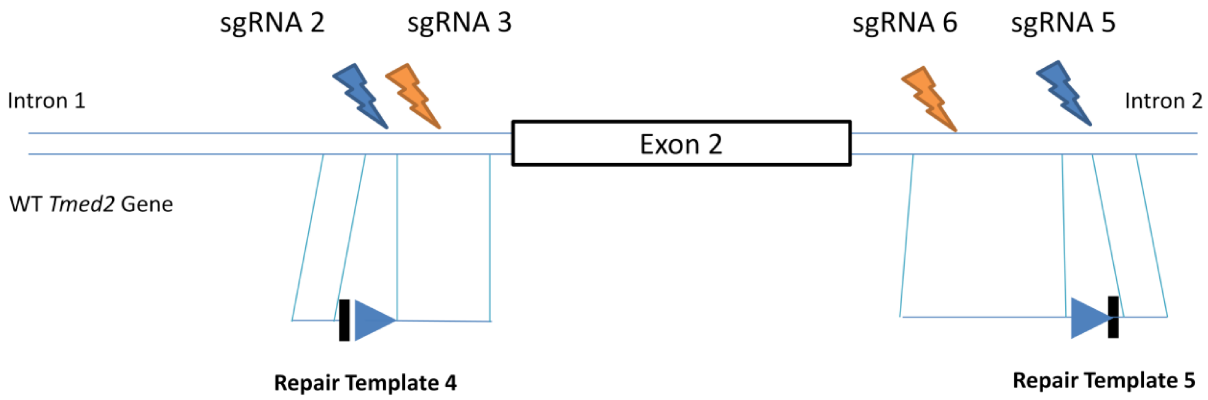

Figure 8 Diagram representing repair templates and sgRNAs used for CRISPR/Cas9 microinjection round 6.

Repair template 4 and 5 are juxtaposed with *Tmed2* exon 2 and surrounding intron 1 and 2 regions to show homologous regions between the repair templates and *Tmed2*. Lightning bolts indicate the *Tmed2* region where the indicated sgRNA is predicted to cut. The black rectangle in the repair templates indicate a restriction site (Repair template (RT) 4= EcoRI; RT 5 = XbaI). The blue triangle in the repair templates indicate a loxP site. All other features in the repair template indicate homologous regions to the wt *Tmed2* gene. For the sequence of each repair template see Table 3.

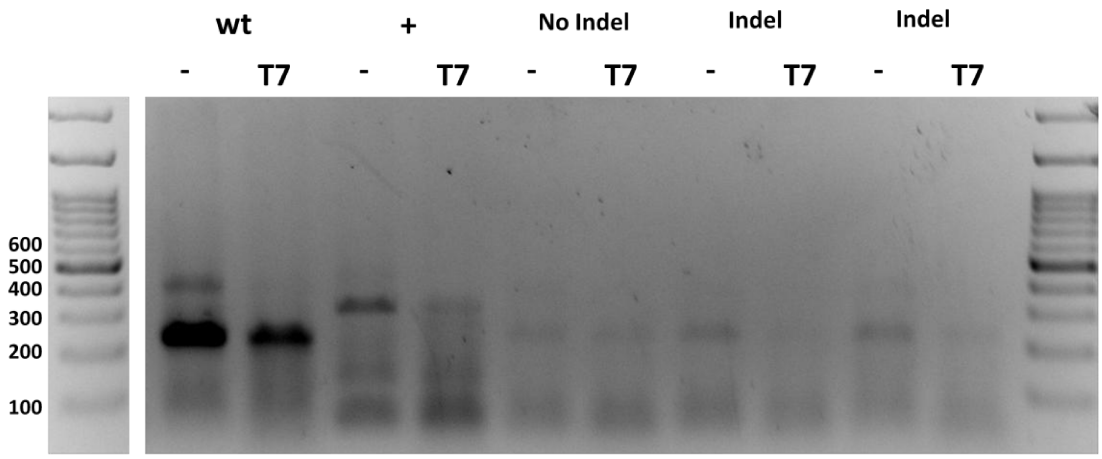

sgRNA (# of blastocysts received)	2 (9)	3 (4)	4 (1)	5 (13)	6 (9)
Indel/Total Screen	6/9 = 67%	3/4 = 75%	1/1 = 100%	4/6 = 67%	4/5 = 80%

Figure 9 T7 endonuclease assay on sgRNA microinjected blastocysts estimates the cutting efficiency of sgRNA 2 thru 6.

Wt sample was a wild-type sample that had not been microinjected with any sgRNA, + control is a sample which carries an insertion event from a non-*Tmed2* micro-injection experiment. - control is the PCR product without T7 endonuclease treatment. T7 is the PCR product treated with T7 endonuclease. "Indel" columns refer to samples which demonstrated positive T7 endonuclease activity, "No Indel" refers to samples which did not demonstrate T7 endonuclease activity. sgRNA 2 and 3 were tested using primers F5R5 and sgRNA 4 thru 6 with primers F6R6.

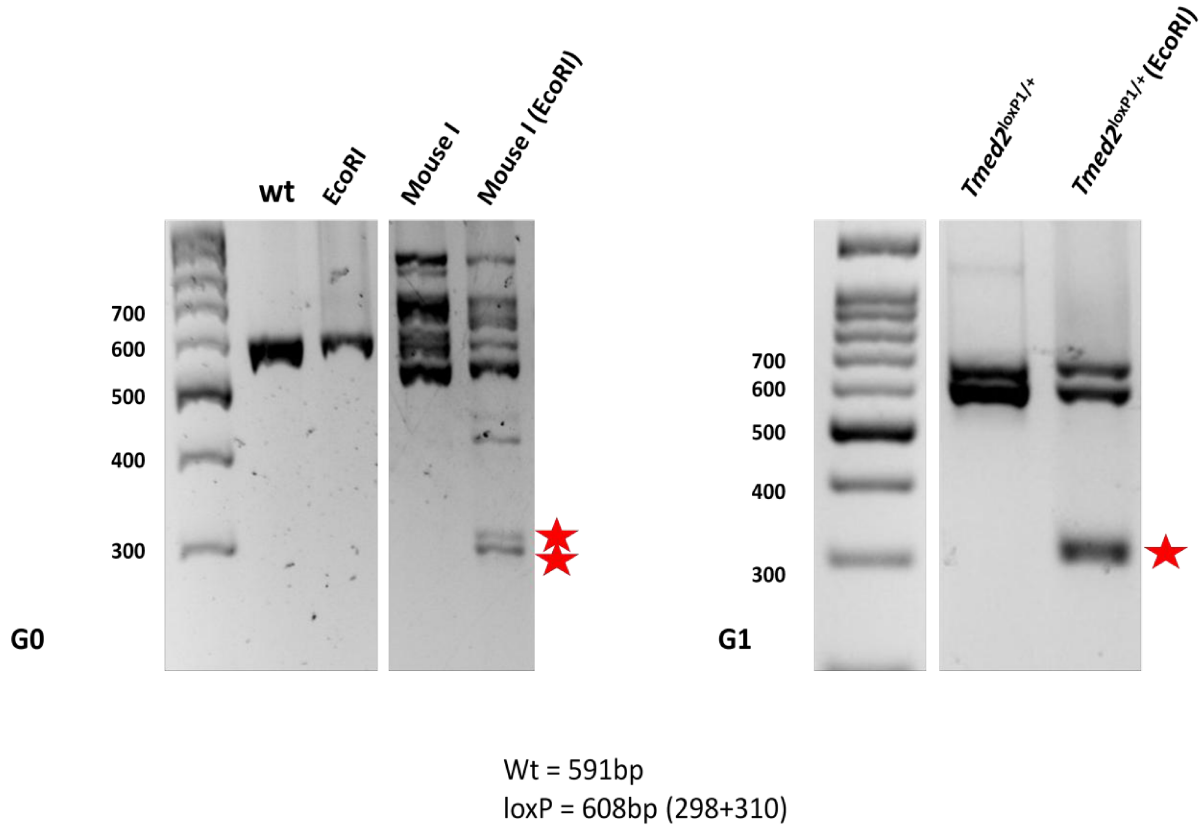

Figure 10 A C3H:Bl6 mouse carries a putative loxP insertion in *Tmed2* intron 1.

Primer pair F2R2 was used to screen *Tmed2* intron 1. Left gel shows the putative *Tmed2* intron 1 loxP carrying C3H:Bl6 (G0) identified as Mouse I. Right gel is representative of screening of mice generated from crossing Mouse I with wt C3H animals which carried the same digestion product as Mouse I. Red stars indicate predicted restriction digestion products following EcoRI digestion of F2R2 PCR products.

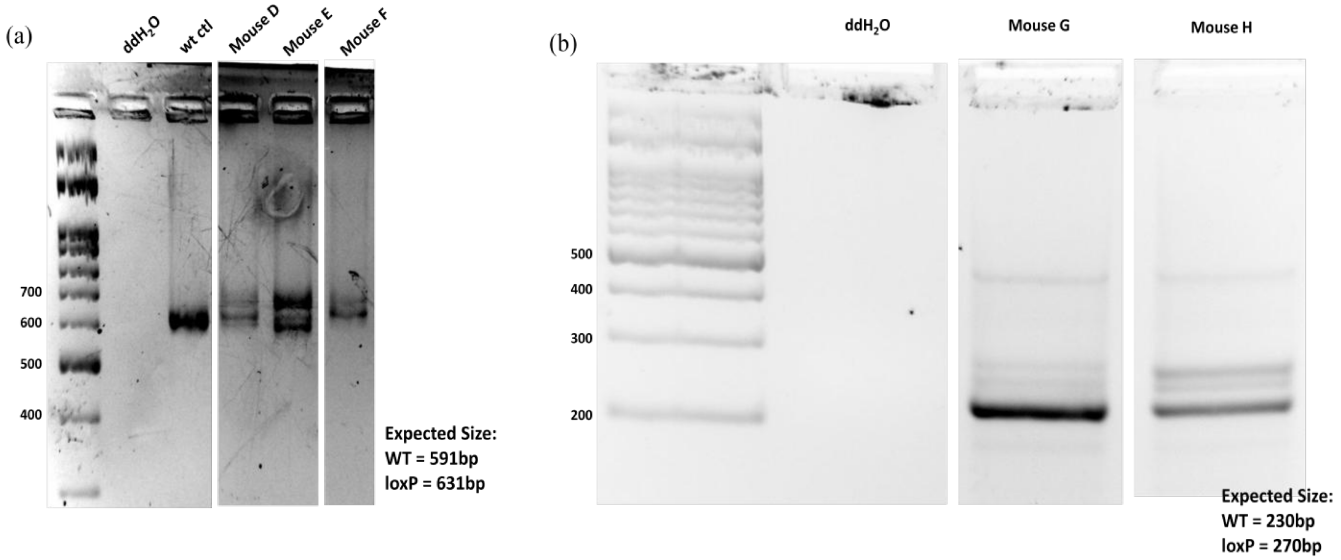

Figure 11 Representative gel electrophoresis of screening for *Tmed2* loxP insertions of C3H:Bl6 CRISPR/Cas9 microinjected mice.

(a) PCR screening using primers F2R2 of C3H:Bl6 mice from CRISPR/Cas9 micro-injected mice for *Tmed2* intron 1 loxP insertion. (b) PCR screening using primers F6R6 of C3H:Bl6 mice from CRISPR/Cas9 micro-injected mice for *Tmed2* intron 2 loxP insertion.

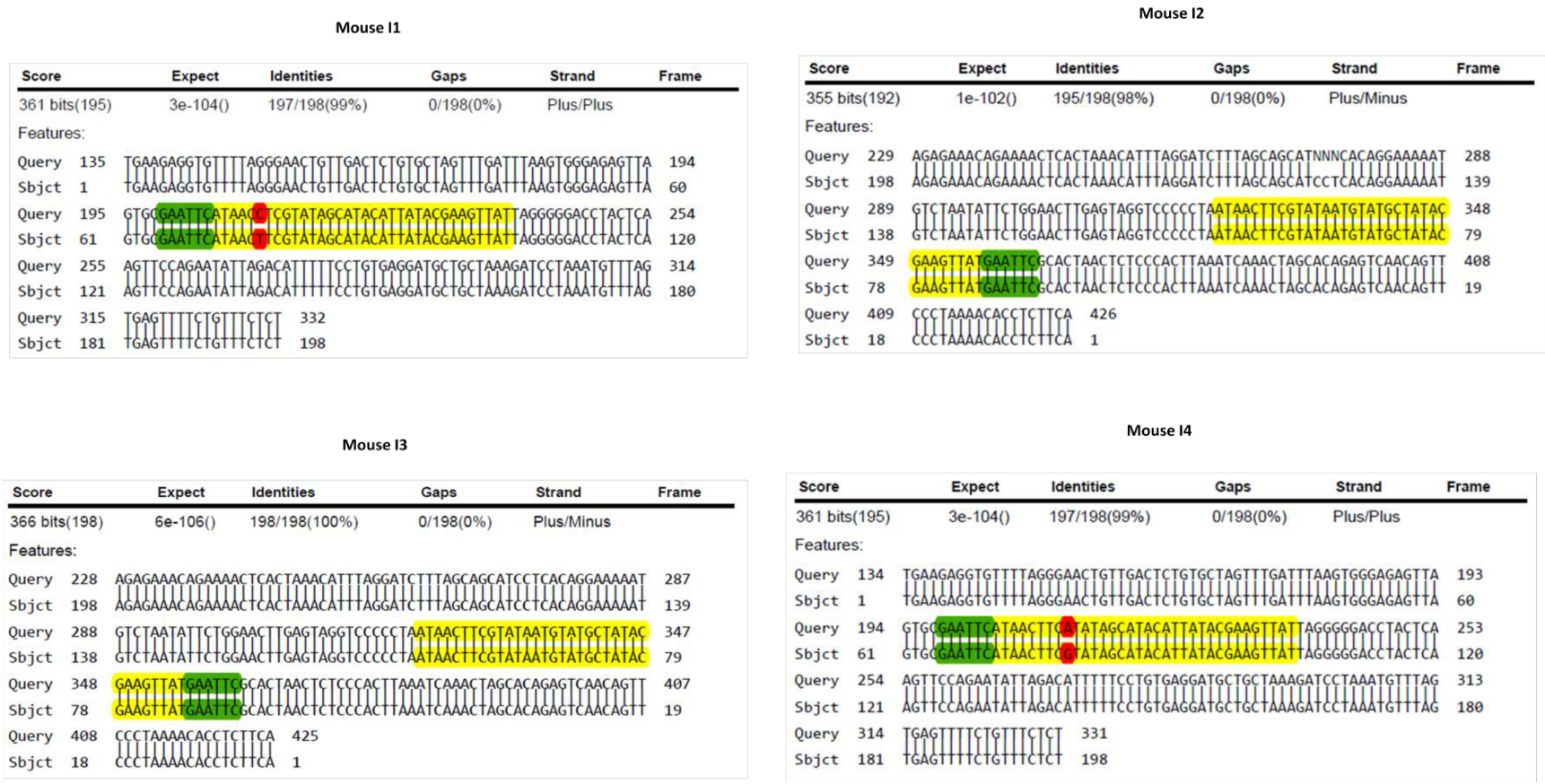

Figure 12 Mouse I offsprings carry the *Tmed2*-loxP1 allele with an intact loxP site.

Displayed are the alignment of the sequencing results (query) for *Tmed2* intron 1 of Mouse I offsprings (I1, 2, 3, 4) to repair template 4 (subject) (see "Table 3"). Highlighted in yellow are the loxP sequences; green, are the restriction digestion site EcoRI; Red are bases that are mismatched representing a mutation in the loxP sequence in the sample.

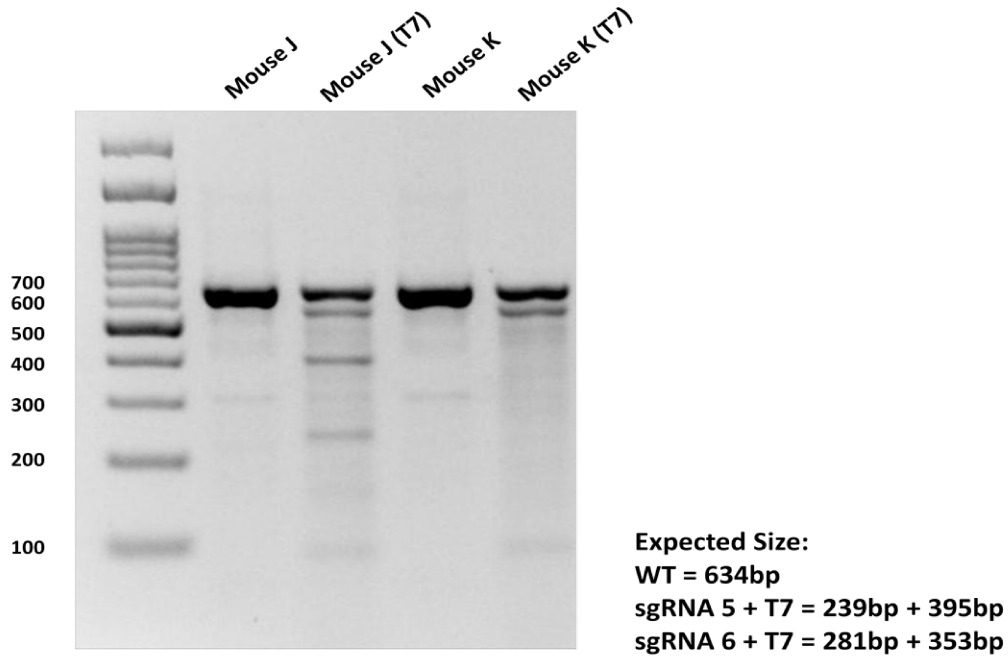

Figure 13 T7 endonuclease on *Tmed2* intron 2 PCR product reveals an indel event in one mouse

Gel electrophoresis of PCR product produced using primer set F4R4 (*Tmed2* intron 2) PCR product-only and T7 endonuclease treated (T7) of two representative samples. Mouse J representates a T7-positive sample and Mouse K a T7-negative sample.

(a)

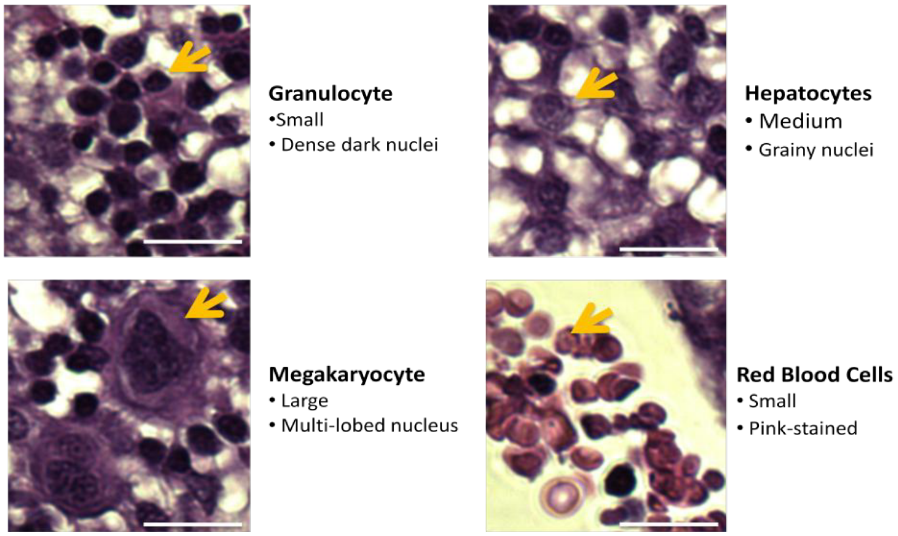

(b)

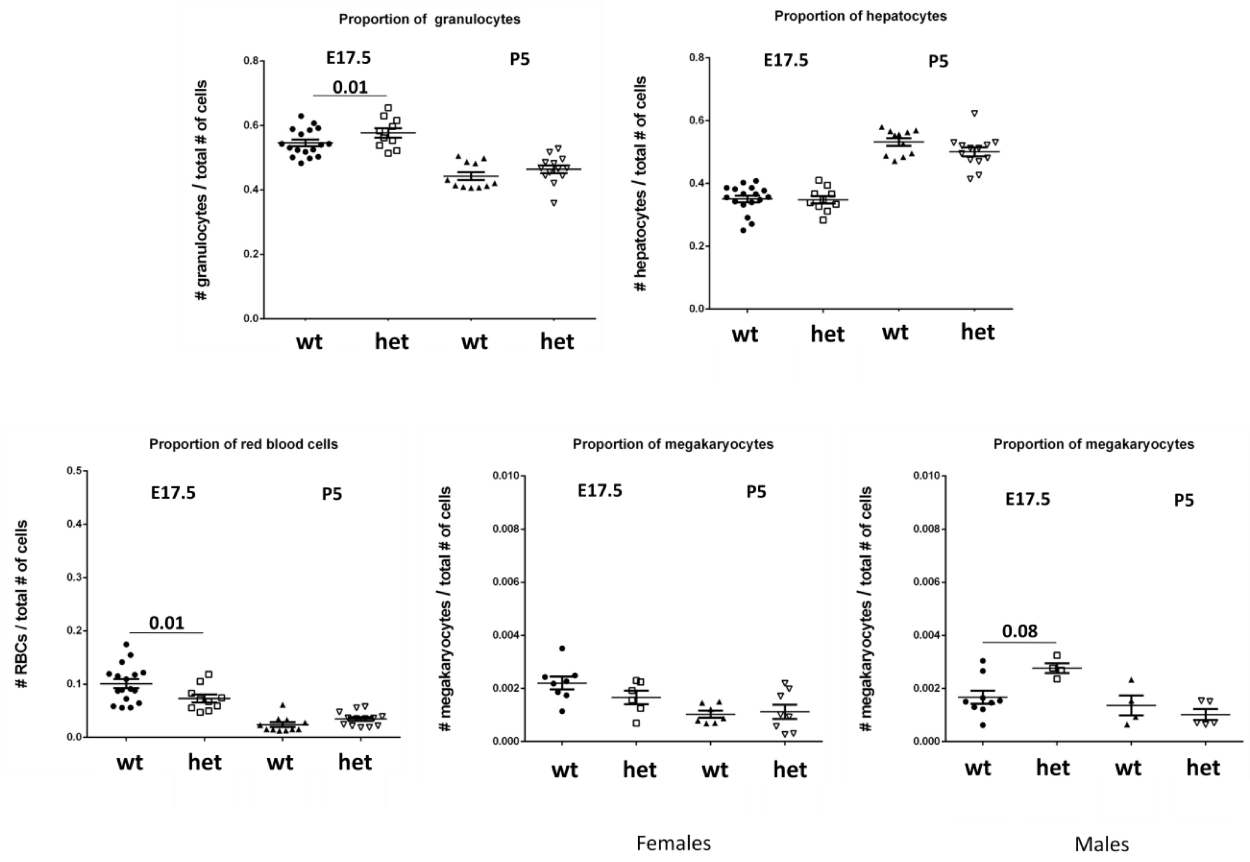

Figure 14 Livers of E17.5 but not P5 *Tmed2*$^{99J/+}$ have deregulated red blood cell and granulocyte proportions.

(a) Images of liver sections stained with HE representing the indicated cell-type (yellow arrow) counted during proportion analysis (Scale bars = 25um). (b) Scatter plot of cell proportions in E17.5 and P5 *Tmed2* wt liver samples compared to *Tmed2*$^{99J/+}$ (het). Statistics used was a two-way ANOVA.

Cell Type	wt (n=4, median)	het (n=5, median)	p-value (Mann-Whitney)
WBC x 10^9/L	5.75	5.2	0.6825
RBC x 10^12/L	6.755	7.83	0.3968

Cell Type	wt (n=4, median)	het (n=4, median)	p-value (Mann-Whitney)
platelets x 10^9/L	628	541	0.2857
neutrophil x 10^9/L	1.485	1.82	0.6571
lymphocytes x 10^9/L	4.16	3.44	0.4857
monocytes x 10^9/L	0	0.05	>0.9999
eosinophils x 10^9/L	0.06	0.075	>0.9999

Figure 15 Peripheral blood cell counts are comparable between 3 month old *Tmed2* wt and *Tmed2*$^{99J/+}$ male mice.

Table of median cell counts obtained from complete blood count anaysis of *Tmed2* wt compared to *Tmed2*$^{99J/+}$ peripheral blood samples. Median values were compared using a Mann-Whitney U test.

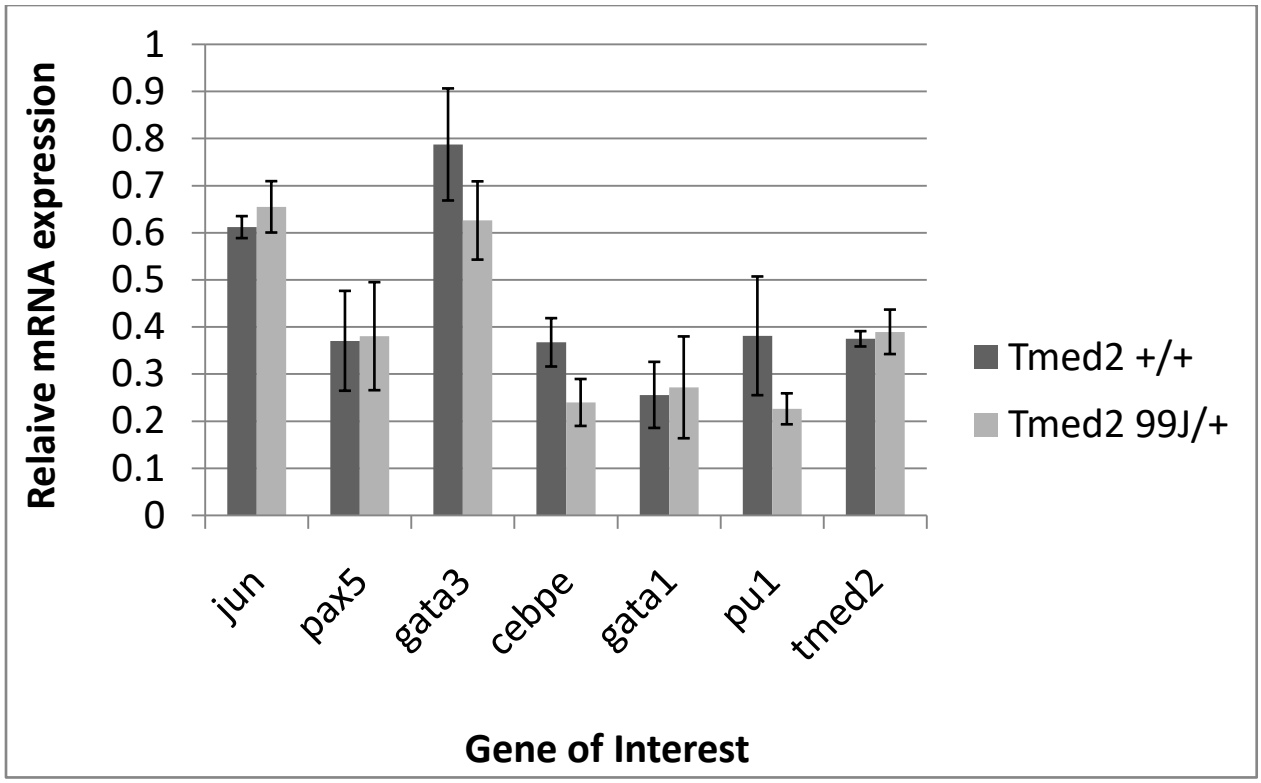

Figure 16 Relative mRNA expression of analyzed hematopoietic transcription factors and of *Tmed2* do not differ between E14.5 livers of *Tmed2* wt and *Tmed2*$^{99J/+}$ embryos.

mRNA expression from RT-qPCR of indicated genes of interest normalized to a normalization factor obtained from expression of internal controls *Actb*, *B2m* and *Sdha*. For *Jun, Pax5* and *Gata-3*, wt n=5 and *Tmed2*$^{99J/+}$ n=5; For *Cebpe, Gata-1, Pu.1* and *Tmed2*, wt n = 3 and *Tmed2*$^{99J/+}$ n=6. Average relative mRNA expressions were compared using a t-test (two-tailed, unpaired); none of the comparisons were statistically significant (i.e. $p>0.05$).

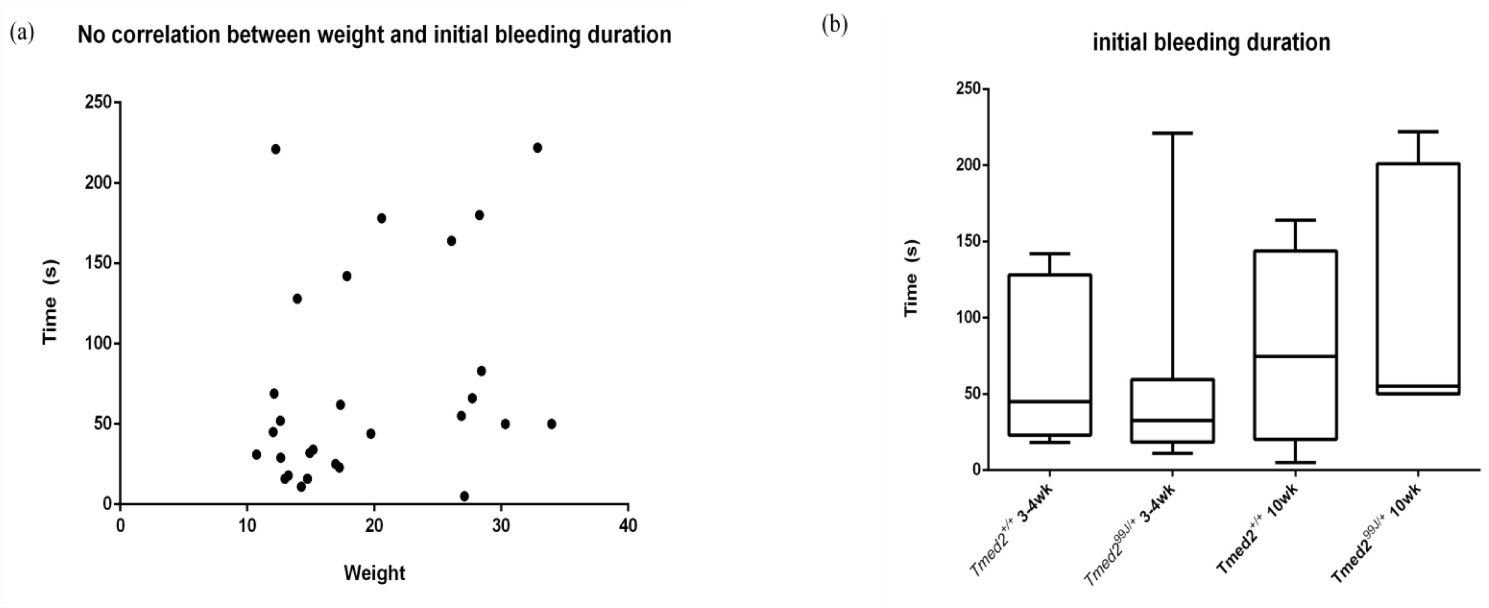

Figure 17 Bleeding duration of 3-4 wks old and 10wk old *Tmed2*$^{99J/+}$ mice are comparable to *Tmed2* wt mice.

(a) Scatter plot of weight of each sample (regardless of age and genotype) against initial bleeding time (seconds). Pearson's correlation coefficient was calculated using GraphPad Prism (R=0.303). (b) Box plot of initial bleeding duration of 3-4wk old (wt, n=7; het, n=12) and 10wk old (wt, n=4; het n=5) *Tmed2* wt compared to *Tmed2*$^{99J/+}$ mice. Initial bleeding durations were compared using using a t-test (two-tailed unpaired), no significant differences were observed.

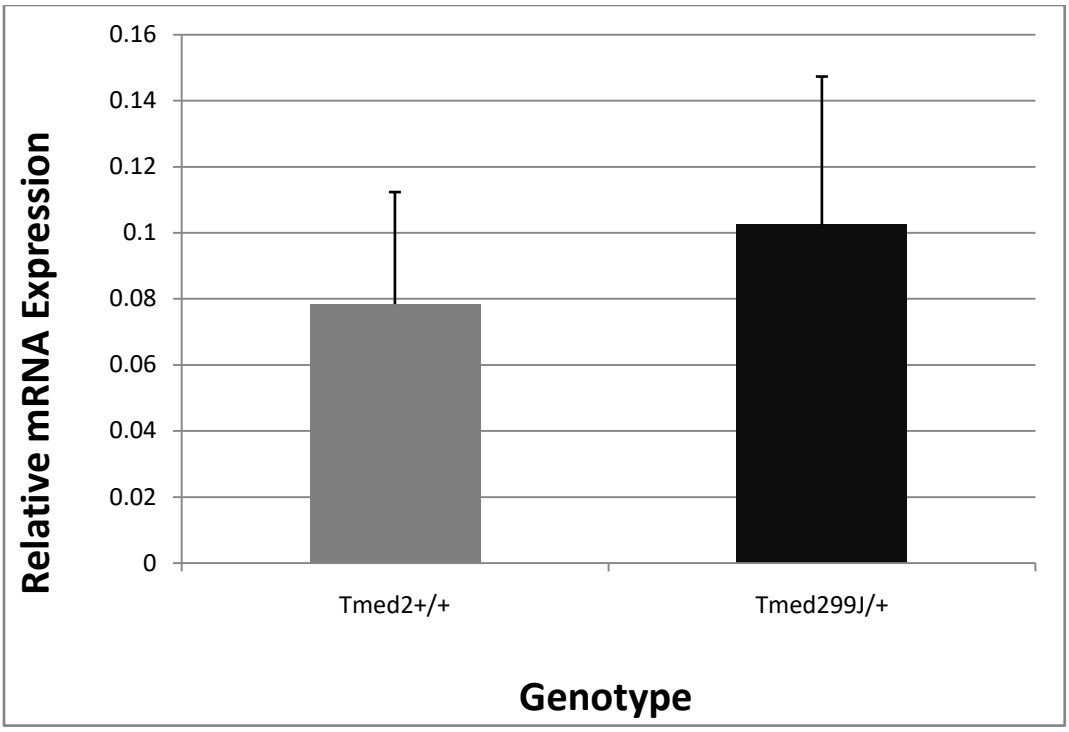

Figure 18 *Par-2* mRNA expression does not differ between *Tmed2* wt and *Tmed2*$^{99J/+}$ E14.5 livers.

mRNA expression from RT-qPCR of *Par-2* normalized to a normalization factor obtained from expression of internal controls *Actb*, *B2m* and *Sdha*. Wt, n=5 and *Tmed2*$^{99J/+}$, n=8. Average relative mRNA expressions were compared using a t-test (two-tailed, unpaired); the difference was not statistically significant (p=0.707).

CHAPTER 6

References

Abremski, K., Hoess, R., Sternberg, N., 1983. Studies on the properties of P1 site-specific recombination: evidence for topologically unlinked products following recombination. Cell 32, 1301-1311.

Adams, E.J., Chen, X.W., O'Shea, K.S., Ginsburg, D., 2014. Mammalian COPII coat component SEC24C is required for embryonic development in mice. The Journal of biological chemistry 289, 20858-20870.

Akira, S., 2000. Roles of STAT3 defined by tissue-specific gene targeting. Oncogene 19, 2607-2611.

Anders, C., Niewoehner, O., Duerst, A., Jinek, M., 2014. Structural basis of PAM-dependent target DNA recognition by the Cas9 endonuclease. Nature 513, 569-573.

Apte, U., Zeng, G., Thompson, M.D., Muller, P., Micsenyi, A., Cieply, B., Kaestner, K.H., Monga, S.P., 2007. beta-Catenin is critical for early postnatal liver growth. American journal of physiology. Gastrointestinal and liver physiology 292, G1578-1585.

Barrangou, R., Fremaux, C., Deveau, H., Richards, M., Boyaval, P., Moineau, S., Romero, D.A., Horvath, P., 2007. CRISPR provides acquired resistance against viruses in prokaryotes. Science 315, 1709-1712.

Basaranoglu, M., Najjar, S.M., Demirbag, A.E., Senturk, H., 2016. Significant cohort of non-alcoholic fatty liver disease with portal vein thrombosis in transplant waiting list. World Journal of Hepatology 8, 376-384.

Behre, G., Whitmarsh, A.J., Coghlan, M.P., Hoang, T., Carpenter, C.L., Zhang, D.E., Davis, R.J., Tenen, D.G., 1999. c-Jun is a JNK-independent coactivator of the PU.1 transcription factor. The Journal of biological chemistry 274, 4939-4946.

Bort, R., Signore, M., Tremblay, K., Barbera, J.P.M., Zaret, K.S., 2006. Hex homeobox gene controls the transition of the endoderm to a pseudostratified, cell emergent epithelium for liver bud development. Developmental Biology 290, 44-56.

Brehm, R., Zeiler, M., Rüttinger, C., Herde, K., Kibschull, M., Winterhager, E., Willecke, K., Guillou, F., Lécureuil, C., Steger, K., Konrad, L., Biermann, K., Failing, K., Bergmann, M., 2007. A sertoli cell-specific knockout of connexin43 prevents initiation of spermatogenesis. The American journal of pathology 171, 19-31.

Buechling, T., Chaudhary, V., Spirohn, K., Weiss, M., Boutros, M., 2011. p24 proteins are required for secretion of Wnt ligands. EMBO reports 12, 1265-1272.

Chen, S., Lee, B., Lee, A.Y., Modzelewski, A.J., He, L., 2016. Highly Efficient Mouse Genome Editing by CRISPR Ribonucleoprotein Electroporation of Zygotes. The Journal of biological chemistry 291, 14457-14467.

Contreras, F.X., Ernst, A.M., Haberkant, P., Björkholm, P., Lindahl, E., Gönen, B.a., Tischer, C., Elofsson, A., von Heijne, G., Thiele, C., Pepperkok, R., Wieland, F., Brügger, B., 2012. Molecular recognition of a single sphingolipid species by a protein's transmembrane domain. Nature Nature 481, 525-529.

Crawford, L.W., Foley, J.F., Elmore, S.A., 2010. Histology atlas of the developing mouse hepatobiliary system with emphasis on embryonic days 9.5-18.5. Toxicol Pathol 38, 872-906.

Delgado, I., Carrasco, M., Cano, E., Carmona, R., García-Carbonero, R.o., Marín-Gómez, L.M., Soria, B., Martín, F., Cano, D.A., Muñoz-Chápuli, R.n., Rojas, A., 2014. GATA4 loss in the septum transversum mesenchyme promotes liver fibrosis in mice. Hepatology 59, 2358-2370.

Diez-Roux, G., Banfi, S., Sultan, M., Geffers, L., Anand, S., Rozado, D., Magen, A., Canidio, E., Pagani, M., Peluso, I., Lin-Marq, N., Koch, M., Bilio, M., Cantiello, I., Verde, R., De Masi, C., Bianchi, S.A., Cicchini, J., Perroud, E., Mehmeti, S., Dagand, E., Schrinner, S., Nurnberger, A., Schmidt, K., Metz, K., Zwingmann, C., Brieske, N., Springer, C., Hernandez, A.M., Herzog, S., Grabbe, F., Sieverding, C., Fischer, B., Schrader, K., Brockmeyer, M., Dettmer, S., Helbig, C., Alunni, V., Battaini, M.A., Mura, C., Henrichsen, C.N., Garcia-Lopez, R., Echevarria, D., Puelles, E., Garcia-Calero, E., Kruse, S., Uhr, M., Kauck, C., Feng, G., Milyaev, N., Ong, C.K., Kumar, L., Lam, M., Semple, C.A., Gyenesei, A., Mundlos, S., Radelof, U., Lehrach, H., Sarmientos, P., Reymond, A., Davidson, D.R., Dolle, P., Antonarakis, S.E., Yaspo, M.L., Martinez, S., Baldock, R.A., Eichele, G., Ballabio, A., 2011. A high-resolution anatomical atlas of the transcriptome in the mouse embryo. PLoS biology 9, e1000582.

Dominguez, M., Dejgaard, K., Füllekrug, J., Dahan, S., Fazel, A., Paccaud, J.P., Thomas, D.Y., Bergeron, J.J., Nilsson, T., 1998. gp25L/emp24/p24 protein family members of the cis-Golgi network bind both COP I and II coatomer. The Journal of cell biology 140, 751-765.

Ema, H., Douagi, I., Cumano, A., Kourilsky, P., 1998. Development of T cell precursor activity in the murine fetal liver. EJI European Journal of Immunology 28, 1563-1569.

Fässler, R., Meyer, M., 1995. Consequences of lack of beta 1 integrin gene expression in mice. Genes & development 9, 1896-1908.

Friedman, A.D., 2002. Transcriptional regulation of granulocyte and monocyte development. Oncogene 21, 3377-3390.

Fujiwara, Y., Browne, C.P., Cunniff, K., Goff, S.C., Orkin, S.H., 1996. Arrested development of embryonic red cell precursors in mouse embryos lacking transcription factor GATA-1. Proceedings of the National Academy of Sciences 93, 12355.

Garbes, L., Kim, K., Riess, A., Hoyer-Kuhn, H., Beleggia, F., Bevot, A., Kim, M.J., Huh, Y.H., Kweon, H.S., Savarirayan, R., Amor, D., Kakadia, P.M., Lindig, T., Kagan, K.O., Becker, J., Boyadjiev, S.A., Wollnik, B., Semler, O., Bohlander, S.K., Kim, J., Netzer, C., 2015. Mutations in SEC24D, encoding a component of the COPII machinery, cause a syndromic form of osteogenesis imperfecta. Am J Hum Genet 96, 432-439.

Godin, I., Garcia-Porrero, J.A., Dieterlen-Lievre, F., Cumano, A., 1999. Stem cell emergence and hemopoietic activity are incompatible in mouse intraembryonic sites. J Exp Med 190, 43-52.

Gommel, D., Orci, L., Emig, E.M., Hannah, M.J., Ravazzola, M., Nickel, W., Helms, J.B., Wieland, F.T., Sohn, K., 1999. p24 and p23, the major transmembrane proteins of COPI-coated transport vesicles, form hetero-oligomeric complexes and cycle between the organelles of the early secretory pathway. FEBS</cja:jid> FEBS Letters 447, 179-185.

Gu, H., Zou, Y.R., Rajewsky, K., 1993. Independent control of immunoglobulin switch recombination at individual switch regions evidenced through Cre-loxP-mediated gene targeting. Cell 73, 1155-1164.

Harvard Stem Cell, I., 2008. Stembook.

Hilberg, F., Aguzzi, A., Howells, N., Wagner, E.F., 1993. c-Jun is essential for normal mouse development and hepatogenesis. Nature 365, 179.

Hou, W., Gupta, S., Beauchamp, M.-C., Yuan, L., Jerome-Majewska, L.A., 2017. Non-alcoholic fatty liver disease in mice with heterozygous mutation in TMED2. PLoS ONE 12, e0182995.

Hsu, P.D., Scott, D.A., Weinstein, J.A., Ran, F.A., Konermann, S., Agarwala, V., Li, Y., Fine, E.J., Wu, X., Shalem, O., Cradick, T.J., Marraffini, L.A., Bao, G., Zhang, F., 2013. DNA targeting specificity of RNA-guided Cas9 nucleases. Nature biotechnology 31, 827-832.

Isern, J., Fraser, S.T., He, Z., Baron, M.H., 2008. The Fetal Liver Is a Niche for Maturation of Primitive Erythroid Cells. procnatiacadscie Proceedings of the National Academy of Sciences of the United States of America 105, 6662-6667.

Jenne, N., Frey, K., Brügger, B., Wieland, F.T., 2002. Oligomeric State and Stoichiometry of p24 Proteins in the Early Secretory Pathway. Journal of Biological Chemistry 277, 46504-46511.

Jerome-Majewska, L.A., Achkar, T., Luo, L., Lupu, F., Lacy, E., 2010. The trafficking protein Tmed2/p24beta(1) is required for morphogenesis of the mouse embryo and placenta. Dev Biol 341, 154-166.

Jinek, M., Chylinski, K., Fonfara, I., Hauer, M., Doudna, J.A., Charpentier, E., 2012. A Programmable Dual-RNA–Guided DNA Endonuclease in Adaptive Bacterial Immunity. Science 337, 816.

Junfeng, H., Ming, Z., Sean, F., Feihan, F.D., Mélanie, R., Alpana, B., Xinyi, H., Weiping, J., Stéphane, A., Michael, B.W., Li, W., 2015. The Identification of Novel Protein-Protein Interactions in Liver that Affect Glucagon Receptor Activity. PLOS ONE 10.

Jung, J., Zheng, M., Goldfarb, M., Zaret, K.S., 1999. Initiation of mammalian liver development from endoderm by fibroblast growth factors. Science (New York, N.Y.) 284, 1988-2003.

Kalies, K.-U., Stokes, V., Hartmann, E., 2008. A single Sec61-complex functions as a protein-conducting channel. Biochimica et Biophysica Acta (BBA) - Molecular Cell Research 1783, 2375-2383.

Koressaar, T., Remm, M., 2007. Enhancements and modifications of primer design program Primer3. Bioinformatics (Oxford, England) 23, 1289-1291.

Kuhn, R., Schwenk, F., Aguet, M., Rajewsky, K., 1995. Inducible gene targeting in mice. Science 269, 1427-1429.

Li, X., Wu, Y., Shen, C., Belenkaya, T.Y., Ray, L., Lin, X., 2015. Drosophila p24 and Sec22 regulate Wingless trafficking in the early secretory pathway. Biochemical and biophysical research communications 463, 483-489.

Long, K.R., Yamamoto, Y., Baker, A.L., Watkins, S.C., Coyne, C.B., Conway, J.F., Aridor, M., 2010. Sar1 assembly regulates membrane constriction and ER export. The Journal of cell biology 190, 115-128.

Luo, W., Wang, Y., Reiser, G., 2007. p24A, a type I transmembrane protein, controls ARF1-dependent resensitization of protease-activated receptor-2 by influence on receptor trafficking. The Journal of biological chemistry 282, 30246-30255.

Luo, W., Wang, Y., Reiser, G., 2011. Proteinase-activated receptors, nucleotide P2Y receptors, and -opioid receptor-1B are under the control of the type I transmembrane proteins p23 and p24A in post-Golgi trafficking. Journal of neurochemistry 117, 71-81.

Ma, X., Chen, C., Veevers, J., Zhou, X., Ross, R.S., Feng, W., Chen, J., 2017. CRISPR/Cas9-mediated gene manipulation to create single-amino-acid-substituted and floxed mice with a cloning-free method. Sci Rep 7, 42244.

Majoul, I., Straub, M., Hell, S.W., Duden, R., Söling, H.D., 2001. KDEL-cargo regulates interactions between proteins involved in COPI vesicle traffic: measurements in living cells using FRET. Developmental cell 1, 139-153.

Makarova, K.S., Haft, D.H., Barrangou, R., Brouns, S.J.J., Charpentier, E., Horvath, P., Moineau, S., Mojica, F.J.M., Wolf, Y.I., Yakunin, A.F., van der Oost, J., Koonin, E.V., 2011. Evolution and classification of the CRISPR–Cas systems. Nature Reviews Microbiology 9, 467.

Malu, K., Garhwal, R., Pelletier, M.G., Gotur, D., Halene, S., Zwerger, M., Yang, Z.F., Rosmarin, A.G., Gaines, P., 2016. Cooperative Activity of GABP with PU.1 or C/EBPepsilon Regulates Lamin B Receptor Gene Expression, Implicating Their Roles in Granulocyte Nuclear Maturation. J Immunol 197, 910-922.

Mancias, J.D., Goldberg, J., 2008. Structural basis of cargo membrane protein discrimination by the human COPII coat machinery. Embo j 27, 2918-2928.

Matsumoto, K., 2001. Liver Organogenesis Promoted by Endothelial Cells Prior to Vascular Function. Science 294, 559-563.

McKercher, S.R., Torbett, B.E., Anderson, K.L., Henkel, G.W., Vestal, D.J., Baribault, H., Klemsz, M., Feeney, A.J., Wu, G.E., Paige, C.J., Maki, R.A., 1996. Targeted disruption of the PU.1 gene results in multiple hematopoietic abnormalities. Embo j 15, 5647-5658.

McMahon, A.P., Bradley, A., 1990. The Wnt-1 (int-1) proto-oncogene is required for development of a large region of the mouse brain. Cell 62, 1073-1085.

Merte, J., Jensen, D., Wright, K., Sarsfield, S., Wang, Y., Schekman, R., Ginty, D.D., 2010. Sec24b selectively sorts Vangl2 to regulate planar cell polarity during neural tube closure. Nature cell biology 12, 41-46; sup pp 41-48.

Mojica, F.J.M., Díez-Villaseñor, C., García-Martínez, J., Almendros, C., 2009. Short motif sequences determine the targets of the prokaryotic CRISPR defence system. Microbiology 155, 733-740.

Nagae, M., Hirata, T., Morita-Matsumoto, K., Theiler, R., Fujita, M., Kinoshita, T., Yamaguchi, Y., 2016. 3D Structure and Interaction of p24beta and p24delta Golgi Dynamics Domains: Implication for p24 Complex Formation and Cargo Transport. J Mol Biol 428, 4087-4099.

Paix, A., Folkmann, A., Goldman, D.H., Kulaga, H., Grzelak, M.J., Rasoloson, D., Paidemarry, S., Green, R., Reed, R.R., Seydoux, G., 2017. Precision genome editing using synthesis-dependent repair of Cas9-induced DNA breaks. Proceedings of the National Academy of Sciences of the United States of America 114, 10745.

Piper, R., Bryant, N., 2009. Posttranslational Control of Protein Trafficking in the Post-Golgi Secretory and Endocytic Pathway, Trafficking Inside Cells : Pathways, Mechanisms and Regulation. New York, NY : Springer New York, pp. 363-387.

Port, F., Basler, K., 2010. Wnt trafficking: new insights into Wnt maturation, secretion and spreading. Traffic (Copenhagen, Denmark) 11, 1265-1271.

Port, F., Hausmann, G., Basler, K., 2011. A genome-wide RNA interference screen uncovers two p24 proteins as regulators of Wingless secretion. EMBO Rep 12, 1144-1152.

Rapoport, T.A., Jungnickel, B., Kutay, U., 1996. Protein Transport Across the Eukaryotic Endoplasmic Reticulum and Bacterial Inner Membranes. Annual Review of Biochemistry 65, 271-303.

Richardson, C.D., Ray, G.J., DeWitt, M.A., Curie, G.L., Corn, J.E., 2016. Enhancing homology-directed genome editing by catalytically active and inactive CRISPR-Cas9 using asymmetric donor DNA. Nature biotechnology 34, 339-344.

Rossi, J.M., Dunn, N.R., Hogan, B.L., Zaret, K.S., 2001. Distinct mesodermal signals, including BMPs from the septum transversum mesenchyme, are required in combination for hepatogenesis from the endoderm. Genes & development 15, 1998-2009.

Sakane, N., Asano, Y., Kawamura, T., Takatani, T., Kohama, Y., Tsujikawa, K., Yamamoto, H., 2004. Aminopeptidase N/CD13 regulates the fetal liver microenvironment of hematopoiesis. Biological & pharmaceutical bulletin 27, 2014-2020.

Sambrook, J., Russell, D.W., 2006. Alkaline agarose gel electrophoresis. CSH protocols 2006.

Sapranauskas, R., Gasiunas, G., Fremaux, C., Barrangou, R., Horvath, P., Siksnys, V., 2011. The Streptococcus thermophilus CRISPR/Cas system provides immunity in Escherichia coli. Nucleic acids research 39, 9275-9282.

Schmidt, C., Bladt, F., Goedecke, S., Brinkmann, V., Zschiesche, W., Sharpe, M., Gherardi, E., Birchmeier, C., 1995. Scatter factor/hepatocyte growth factor is essential for liver development. Nature 373, 699-702.

Segev, N., 2009. Trafficking inside cells : pathways, mechanisms, and regulation.

Serls, A.E., Doherty, S., Parvatiyar, P., Wells, J.M., Deutsch, G.H., 2005. Different thresholds of fibroblast growth factors pattern the ventral foregut into liver and lung. Development 132, 35.

Shibata, M., Nishimasu, H., Kodera, N., Hirano, S., Ando, T., Uchihashi, T., Nureki, O., 2017. Real-space and real-time dynamics of CRISPR-Cas9 visualized by high-speed atomic force microscopy. Nature Communications 8, 1430.

Sokol, S.Y., 2015. Spatial and temporal aspects of Wnt signaling and planar cell polarity during vertebrate embryonic development. Seminars in Cell & Developmental Biology 42, 78-85.

Soriano, P., 1999. Generalized lacZ expression with the ROSA26 Cre reporter strain. Nature Genetics 21, 70.

Sosa-Pineda, B., Wigle, J.T., Oliver, G., 2000. Hepatocyte migration during liver development requires Prox1. Nature genetics 25, 254-255.

Spang, A., 2002. ARF1 regulatory factors and COPI vesicle formation. COCEBI</cja:jid> Current Opinion in Cell Biology 14, 423-427.

Stagg, S.M., Gürkan, C., Fowler, D.M., LaPointe, P., Foss, T.R., Potter, C.S., Carragher, B., Balch, W.E., 2006. Structure of the Sec13/31 COPII coat cage. Nature 439, 234-238.

Stepanchick, A., Breitwieser, G.E., 2010. The cargo receptor p24A facilitates calcium sensing receptor maturation and stabilization in the early secretory pathway. Biochemical and biophysical research communications 395, 136-140.

Sternberg, N., Hamilton, D., 1981. Bacteriophage P1 site-specific recombination:I. Recombination between loxP sites. YJMBI</cja:jid> Journal of Molecular Biology 150, 467-486.

Stirling, C.J., Rothblatt, J., Hosobuchi, M., Deshaies, R., Schekman, R., 1992. Protein translocation mutants defective in the insertion of integral membrane proteins into the endoplasmic reticulum. Molecular biology of the cell 3, 129-142.

Strating, J., Bakel, v.N.H.M., Leunissen, J.A.M., Martens, G.J.M., 2009. Comprehensive overview of the vertebrate p24 family: identification of a novel tissue-specifically expressed member. Molecular Biology and Evolution 26, 1707-1714.

Summer, H., Grämer, R., Dröge, P., 2009. Denaturing Urea Polyacrylamide Gel Electrophoresis (Urea PAGE). Journal of Visualized Experiments : JoVE, 1485.

Swarup, S., Verheyen, E.M., 2012. Wnt/Wingless Signaling in Drosophila. Cold Spring Harbor Perspectives in Biology 4, a007930.

Takayuki, S., Satoshi, W., Akiko, K., Masahiro, S., Takayuki, S., 2014. A single blastocyst assay optimized for detecting CRISPR/Cas9 system-induced indel mutations in mice. BMC Biotechnology 14, 69.

Tan, X., Yuan, Y., Zeng, G., Apte, U., Thompson, M.D., Cieply, B., Stolz, D.B., Michalopoulos, G.K., Kaestner, K.H., Monga, S.P.S., 2008. β-Catenin deletion in hepatoblasts disrupts hepatic morphogenesis and survival during mouse development. HEP Hepatology 47, 1667-1679.

Theiler, R., Fujita, M., Maeda, Y., Kinoshita, T., Nagae, M., Yamaguchi, Y., Fujita, M., 2014. The α-helical region in p24γ2 subunit of p24 protein cargo receptor is pivotal for the recognition and transport of glycosylphosphatidylinositol-anchored proteins. J. Biol. Chem. Journal of Biological Chemistry 289, 16835-16843.

Ting, C.N., Olson, M.C., Barton, K.P., Leiden, J.M., 1996. Transcription factor GATA-3 is required for development of the T-cell lineage. Nature 384, 474-478.

Untergasser, A., Cutcutache, I., Koressaar, T., Ye, J., Faircloth, B.C., Remm, M., Rozen, S.G., 2012. Primer3--new capabilities and interfaces. Nucleic acids research 40.

Vandesompele, J., De Preter, K., Pattyn, F., Poppe, B., Van Roy, N., De Paepe, A., Speleman, F., 2002. Accurate normalization of real-time quantitative RT-PCR data by geometric averaging of multiple internal control genes. Genome Biol 3, Research0034.

Visel, A., Thaller, C., Eichele, G., 2004. GenePaint.org: an atlas of gene expression patterns in the mouse embryo. Nucleic Acids Res 32, D552-556.

Walter, P., Johnson, A.E., 1994. Signal Sequence Recognition and Protein Targeting to the Endoplasmic Reticulum Membrane. Annual Review of Cell Biology 10, 87-119.

Wang, H., Yang, H., Shivalila, C.S., Dawlaty, M.M., Cheng, A.W., Zhang, F., Jaenisch, R., 2013. One-Step Generation of Mice Carrying Mutations in Multiple Genes by CRISPR/Cas-Mediated Genome Engineering. Cell 153, 910-918.

Wang, L., Shao, Y., Guan, Y., Li, L., Wu, L., Chen, F., Liu, M., Chen, H., Ma, Y., Ma, X., Liu, M., Li, D., 2015. Large genomic fragment deletion and functional gene cassette knock-in via Cas9 protein mediated genome editing in one-cell rodent embryos. Scientific Reports 5, 17517.

Watt, A.J., Zhao, R., Li, J., Duncan, S.A., 2007. Development of the mammalian liver and ventral pancreas is dependent on GATA4, BioMed Central Ltd. BioMed Central Ltd. 2007-04-23.

Weisend, C.M., Kundert, J.A., Suvorova, E.S., Prigge, J.R., Schmidt, E.E., 2009. Cre activity in fetal albCre mouse hepatocytes: Utility for developmental studies. Genesis 47, 789-792.

Welniak, L.A., Karas, M., Yakar, S., Anver, M.R., Murphy, W.J., LeRoith, D., 2004. Effects of organ-specific loss of insulin-like growth factor-I production on murine hematopoiesis11The content of this publication does not necessarily reflect the views or policies of the Department of Health and Human Services, nor does mention of trade names, commercial products, or organizations imply endorsement by the US government. Biology of Blood and Marrow Transplantation 10, 32-39.

Wen, C., Greenwald, I., 1999. p24 Proteins and Quality Control of LIN-12 and GLP-1 Trafficking in Caenorhabditis elegans. The Journal of Cell Biology 145, 1165-1175.

Wenyang, H., Swati, G., Marie-Claude, B., Libin, Y., Loydie, A.J.-M., 2017. Non-alcoholic fatty liver disease in mice with heterozygous mutation in TMED2. PLOS ONE 12.

Williams, S.C., Du, Y., Schwartz, R.C., Weiler, S.R., Ortiz, M., Keller, J.R., Johnson, P.F., 1998. C/EBPepsilon is a myeloid-specific activator of cytokine, chemokine, and macrophage-colony-stimulating factor receptor genes. The Journal of biological chemistry 273, 13493-13501.

Xu, H., Xiao, T., Chen, C.-H., Li, W., Meyer, C.A., Wu, Q., Wu, D., Cong, L., Zhang, F., Liu, J.S., Brown, M., Liu, X.S., 2015. Sequence determinants of improved CRISPR sgRNA design. Genome Res. Genome Research 25, 1147-1157.

Yakar, S., Liu, J.-L., Stannard, B., Butler, A., Accili, D., Sauer, B., LeRoith, D., 1999. Normal growth and development in the absence of hepatic insulin-like growth factor I. Proceedings of the National Academy of Sciences of the United States of America 96, 7324-7329.

Yang, H., Wang, H., Shivalila, Chikdu S., Cheng, Albert W., Shi, L., Jaenisch, R., 2013. One-Step Generation of Mice Carrying Reporter and Conditional Alleles by CRISPR/Cas-Mediated Genome Engineering. Cell 154, 1370-1379.

Yen, S.-T., Zhang, M., Deng, J.M., Usman, S.J., Smith, C.N., Parker-Thornburg, J., Swinton, P.G., Martin, J.F., Behringer, R.R., 2014. Somatic mosaicism and allele complexity induced by CRISPR/Cas9 RNA injections in mouse zygotes. Developmental biology 393, 3-9.

Yorimitsu, T., Sato, K., Takeuchi, M., 2014. Molecular mechanisms of Sar/Arf GTPases in vesicular trafficking in yeast and plants. Frontiers in Plant Science 5.

Zhao, R., Watt, A.J., Li, J., Luebke-Wheeler, J., Morrisey, E.E., Duncan, S.A., 2005. GATA6 is essential for embryonic development of the liver but dispensable for early heart formation. Molecular and cellular biology 25, 2622-2631.